Multiscale Experimental Mechanics of Hierarchical Carbon-Based Materials

Horacio D. Espinosa, Tobin Filleter, and Mohammad Naraghi*

Investigation of the mechanics of natural materials, such as spider silk, abalone shells, and bone, has provided great insight into the design of materials that can simultaneously achieve high specific strength and toughness. Research has shown that their emergent mechanical properties are owed in part to their specific self-organization in hierarchical molecular structures, from nanoscale to macroscale, as well as their mixing and bonding. To apply these findings to manmade materials, researchers have devoted significant efforts in developing a fundamental understanding of multiscale mechanics of materials and its application to the design of novel materials with superior mechanical performance. These efforts included the utilization of some of the most promising carbon-based nanomaterials, such as carbon nanotubes, carbon nanofibers, and graphene, together with a variety of matrix materials. At the core of these efforts lies the need to characterize material mechanical behavior across multiple length scales starting from nanoscale characterization of constituents and their interactions to emerging micro- and macroscale properties. In this report, progress made in experimental tools and methods currently used for material characterization across multiple length scales is reviewed, as well as a discussion of how they have impacted our current understanding of the mechanics of hierarchical carbon-based materials. In addition, insight is provided into strategies for bridging experiments across length scales, which are essential in establishing a multiscale characterization approach. While the focus of this progress report is in experimental methods, their concerted use with theoretical-computational approaches towards the establishment of a robust material by design methodology is also discussed, which can pave the way for the development of novel materials possessing unprecedented mechanical properties.

1. Introduction

Nature utilizes self-organized hierarchical structures, which exhibit extraordinary stiffness, strength and toughness with low weight, to accomplish a vast number of functions. These structures range from internal components such as mammalian bone and tendons, to protective elements such as seashell nacre, to external survival tools such as spider silks. Research has shown that the superior mechanical behavior of all of these materials rely intimately on their hierarchical structures.[1–8] New research efforts are increasingly being developed to apply these lessons from nature toward the development of artificial materials that can achieve a similar marriage of strength and toughness such as synthetic composites that emulate nacre, and bioinspired fibers that emulate spider silk.[9,10]

In particular, the application of crystalline 1D and 2D carbon-based materials, such as carbon nanotubes (CNT) and graphene, as building blocks in artificial hierarchical structures has received a great deal of attention. The unique sp^2 in-plane carbon bonding found in CNTs and graphene sheets yields some of the stiffest and strongest materials known to man. Recent experiments on both CNTs and graphene have confirmed theoretical predictions, and demonstrated elastic moduli of up to 1 TPa and strengths of over 100 GPa.[11–13] These proven intrinsic mechanical properties have sparked the questions of whether these materials can be organized in hierarchical structures to achieve performance even superior to naturally occurring materials. In the case of CNTs, their 1D nature is envisioned to act as a building block in engineered fibers akin to the mineralized collagen fibrils found in tendon. Alternatively, the 2D nature of graphene sheets can be used to mimic the aragonite platelets found in the layered structure of nacre.[2] While the intrinsic properties of these carbon-based building blocks is well understood, a great deal of work is required to understand and engineer how they can be effectively assembled to emulate the complex hierarchical structures of natural materials.

One of the fundamental challenges to assemble carbon-based materials into high performance hierarchical structures is engineering their interfacial interactions across multiple scales. In the natural case of tendons, the structure is organized in seven hierarchical levels with different interaction mechanisms acting at each level (see **Figure 1**a).[14,15] At the first level, tropocollagen

Prof. H. D. Espinosa, Dr. T. Filleter, Dr. M. Naraghi[+]
Department of Mechanical Engineering
Northwestern University
2145 Sheridan Rd., Evanston, IL 60208-3111, USA
E-mail: espinosa@northwestern.edu
[+] Present Address: Department of Aerospace Engineering, Texas A &M University, 3141 TAMU, College Station, TX 77843-3141, USA

DOI: 10.1002/adma.201104850

molecules consist of three polypeptides arranged in a triple helix bonded together laterally via hydrogen bonding (H-bonding). Upon tensile loading, the H-bonds rupture in a reversible process yielding a mechanism allowing the collagen fibrils to deform up to 50% prior to failure while dissipating energy.[1,16] On the larger scales, collagen fibrils are organized into arrays connected by a biopolymer phase, which provides additional energy dissipation mechanisms. These different interfacial interactions at multiple length scales collectively contribute to the macroscopic toughness of tendons. Recent modeling shows that these interfacial interactions follow length scales associated to the interface geometry and chemical bonds.[17] A similarly complex hierarchical structure with varying interfacial interactions is also found in spider silk and nacre. An overarching mechanism that is common between these natural materials is a tolerance to flaws. In silk, it has been shown that macroscopic fibers and bundles can have high strength and toughness as a result of the delocalization of stress concentrators at scales of ~100 nm.[8,10] In nacre, the brick-and-mortar-like microstructure allows for damage propagation over millimeter length scales dramatically increasing toughness.[9] Similarly, engineering interfacial interactions across hierarchical length scales and the utilization of toughening mechanisms is required in order to develop tough macroscopic materials out of CNT (see Figure 1b) and graphene building blocks, which are otherwise inherently brittle. To address this challenge, there is a great need for characterization and testing of mechanical properties and shear interactions across multiple length scales. This need has sparked a new multiscale approach to understanding the mechanics of carbon-based materials which merges established nanomechanical testing such as atomic force microscopy (AFM), in situ micro-electrical-mechanical systems (MEMS) based testing, in situ Raman spectroscopy testing, and classical micromechanical testing methods. Only through application of such methods, and addressing each length scale in the hierarchical structure, can novel carbon-based materials be designed to emulate and surpass the properties of natural materials.

The envisioned carbon-based materials have the potential to make a significant impact, in particular on aerospace and military applications, which utilize fiber reinforced structural composites and armor structures. Hierarchical CNT based fibers are emerging as a class of material proposed to replace more traditional high strength carbon fibers in composite materials.[18–23] In addition to applications requiring high performance in mechanical properties, CNT fibers and sheets are also being applied as templates to develop multifunctional materials[24] and temperature-invariant artificial muscles.[25] For example, Lima et al., have recently developed a bi-scrolling method of fabricating composite yarns based on the spinning method of CNTs from forests, in which drawn sheets of CNTs are used as hosts of otherwise unspinnable powders and granulates to develop multifunctional yarns suitable for high tech applications, such as superconductors and flexible battery cathodes.[24]

Macroscopic graphene composites and graphene oxide based materials are also beginning to emerge,[26,27] however initial implementations are yet to approach the intrinsic superior mechanical properties of the building block constituents. The gap between the mechanical properties of the composites and their nanometer size building blocks further emphasizes the great need for a better multiscale understanding of how the hierarchical structures and interactions at multiple levels within the materials play a role in the macroscopic behavior. We envision that this will ultimately be achieved in great part by the development and application of unique experimental tools to

Horacio Espinosa is the director of the Theoretical and Applied Mechanics program, and the James and Nancy Farley Professor in the Department of Mechanical Engineering at Northwestern University. He received his PhD degree from Brown University in 1992. Professor Espinosa has made contributions in the areas of dynamic failure of advanced materials, computational modeling of fracture, and multiscale experiments and simulations of micro- and nano-systems. He has published over 200 technical papers in these fields.

Tobin Filleter is a Postdoctoral Fellow in the Department of Mechanical Engineering at Northwestern University under the supervision of Professor Espinosa. He received his PhD from McGill University in 2009. His research interests include nanomechanics of advanced materials, nanotribology and atomic-scale friction, in situ MEMS based SEM/TEM mechanical testing, multiscale experiments of nanosystems, and the mechanics of graphene and CNTs.

Mohammad Naraghi received his PhD from University of Illinois at Urbana-Champaign in 2009. From 2009 to 2011 he worked as a post-doctorate research fellow under the supervision of Professor Espinosa in Northwestern University. Since 2012, he is an assistant professor in Texas A & M University, department of Aerospace engineering. His research expertise is in nanomechanics, application of MEMS for the characterization of nanomaterials, and the development of bio-inspired lightweight novel materials.

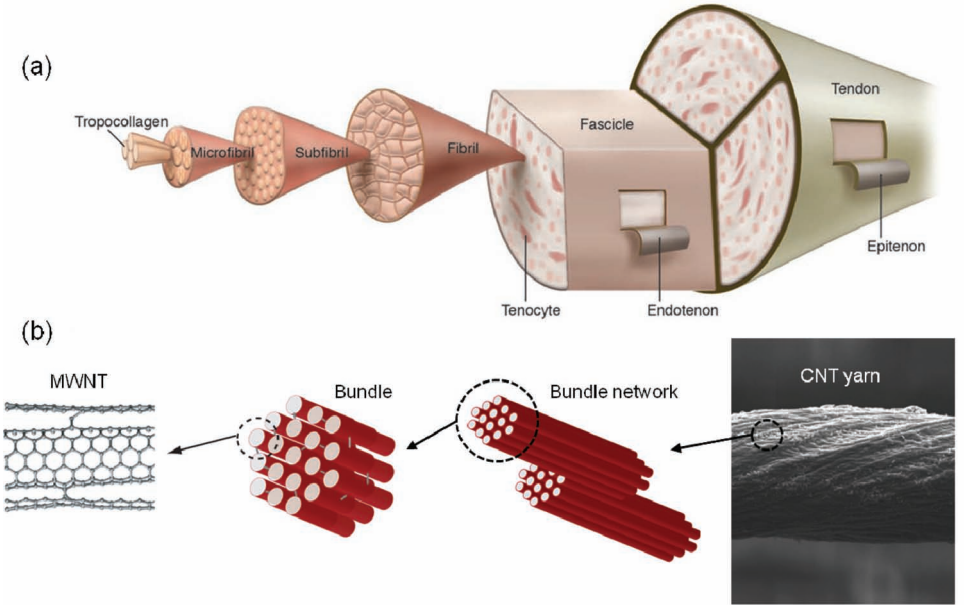

Figure 1. (a) Schematic representation of the multiple levels of the hierarchical structure found in natural tendons. Reproduced with permission,[14] Copyright 2008, American Society for Clinical Investigation. (b) SEM image of a Carbon nanotube yarn (far right) including a schematic representation of its hierarchical structure across multiple length scales.

enable the understanding of deformation mechanisms at each length scale.

2. Multiscale Experimental Tools

Elucidating a complete understanding of the mechanical properties and behavior of carbon-based composite materials requires a diverse tool box of techniques which can not only resolve the forces acting at each hierarchical level, but also reveal deformation and failure of the structures at each scale. While it has become common place to identify strain and failure at macro and microscopic scales through optical techniques, it has only been in the last few decades that novel techniques have been developed to characterize mechanical behavior at the nanoscale. This has been, in the most part, enabled by the application of two revolutionary approaches to the study of mechanics; atomic force microscopy (AFM) and in situ scanning and transmission electron microscopy (in situ SEM and TEM). Together these two techniques have addressed the most fundamental requirements for studying mechanics of nanoscale constituents such as CNTs and graphene sheets; namely, (1) the capability to measure forces in the range of pico to nanoNewtons, and (2) real space imaging resolution extending down to individual atoms. Although these approaches have already yielded a great deal of understanding of individual CNT and graphene properties, they are only beginning to address characterization at higher scales in carbon-based materials such as the shear interactions between adjacent nanoscale constituents. This level in the hierarchy of carbon-based composites remains one of the biggest bottle necks impeding the development of high performance macroscopic materials. This has initiated the application of additional experimental techniques, such as Raman spectroscopy and nanoindentation, to characterize interactions and local mechanical behavior of the constituents within larger networks. When coupled with more traditional micromechanical testing methods, this combination of techniques will be essential in moving forward the frontiers of multiscale experiments on carbon-based materials. As an example, **Table 1** outlines the different hierarchical levels in CNT yarns and details the above mentioned experimental tools as well as modeling techniques which can be applied at each length scale.

2.1. Revealing Atomic Level Mechanics: in situ TEM Methods

TEM has become one of the most powerful tools to characterize the real space atomic level structure of a wide variety of materials. With the application to low dimension carbon materials it has been particularly useful, most notably facilitating the discovery of CNTs by Ijima[31] and revealing the nature of defects in CNTs and graphene through direct atomic resolution imaging.[12,32] The latter accomplishment epitomizes one of the greatest strengths of TEM: local Ångstrom-level spatial resolution, which can be achieved due to the relatively small wavelengths of high energy electrons used to probe the sample. In addition, such atomic-scale imaging is not limited to surfaces (information related to the real space) and can be combined with electron diffraction (information related to the reciprocal space) giving TEM a very unique capability. These strengths of TEM coupled with the need to understand the mechanical behavior of emerging nanomaterials initiated a new field in mechanics that aimed at conducting mechanical testing of nanostructures with near real time observation of their deformation and failure: in situ TEM mechanical testing. Initial work in the field utilized tensile straining holders and nanomanipulators, providing

Table 1. Multiscale experimental and theoretical modeling approaches applied to study hierarchical carbon nanotube based fiber materials.

Length Scale	Single CNT Level (Å - nm)	CNT Bundle Level (nm – µm)	Bundle Network Level (µm – 10's µm)	CNT Yarn Level (10's µm – mm)
	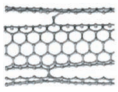	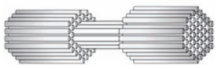		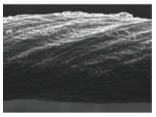
Experiment	In-situ TEM, MEMS-based mechanical testing, Selected area electron diffraction (SAED) 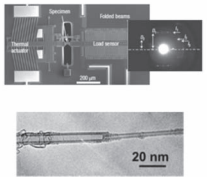	Atomic Force Microscopy (AFM), MEMS-based mechanical testing, CNT pullout measurements 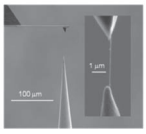	In-situ Raman Spectroscopy, Shear force measurements, Peeling experiments using micro cantilevers 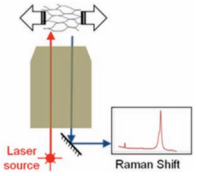	In-situ SEM Micromechanical testing, Dynamic Mechanical Analysis (DMA), Nanoindentation 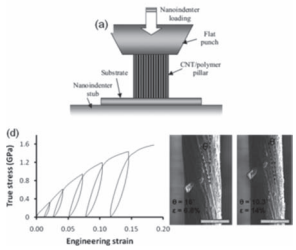
Modeling	Density Functional Theory (DFT and DFTB) and Molecular Mechanics/Dynamics	Molecular Dynamics, Molecular Mechanics, and Coarse-grain MD	Coarse-grain Molecular Dynamics and Continuum Shear-lag	Continuum Shear-lag, Finite element, and Analytical models
Parametric Identification	• Elastic modulus, E, and strength, σ, of CNT shells • CNT shell-shell shear strength • Load transfer fraction between CNT shells • Cohesion energy	• Effective modulus, E, & strength, σ, of CNT bundles • Shear force between close packed CNTs • Cohesion energy	• Shear strength and shear modulus of bundle-bundle interface • Local CNT strain in CNT bundle network	• Elastic modulus, E, strength, σ, and energy-to-failure of yarns • Storage and Loss modulus

Single CNT level,[28] adapted with permission from AAAS,[12] and Macmillan Publishers Ltd: Nature Nanotechnology, Copyright 2008. *CNT bundle level*, adapted with permission from [76] Copyright (2010) American Chemical Society. *Bundle network level*, adapted from.[29] *CNT yarn level*, adapted with permission from [23] Copyright (2010) American Chemical Society, and adapted from [30].

important initial findings on dislocation based plasticity and failure mechanisms in a variety of materials.[33] In the case of CNTs, nanomanipulation in situ TEM allowed visualization of the sword-in-sheath failure mechanism in which adjacent multi-wall carbon nanotube (MWNT) shells slide with respect to one another due to weak shear interactions (see **Figure 2**a),[12,28] demonstrating one of the central limitations in scaling individual CNT shell mechanical properties to macroscopic

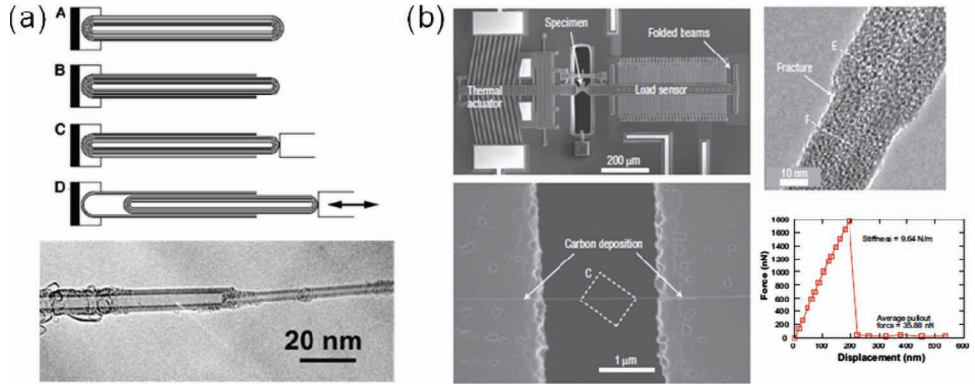

Figure 2. (a) In situ TEM nanomanipulation of a MWNT revealing sword-in-sheath failure in which inner CNT shells pullout with respect to outer shells. (Top) Schematic representation of the MWNT manipulation. (Bottom) HRTEM image of a MWNT after manipulation. Reprinted with permission from AAAS.[28] (b) MEMS based in situ TEM uniaxial tensile testing of a MWNT. (Left) The top SEM image shows a MEMS based tensile testing device and the bottom image shows a MWNT suspending the device. (Right) The top shows a HRTEM image of a MWNT after tensile testing (adapted with permission from Macmillan Publishers Ltd: Nature Nanotechnology,[12] copyright 2008) and the bottom show a force-displacement curve during tensile testing. Adapted with permission,[39] copyright 2009, SEM.

materials. While these techniques have been effective in visualizing mechanical deformation and failure, they are limited in that they do not allow for the simultaneous measurement of forces. This limitation was overcome by the use of MEMS technologies.[34–36] In its most advanced version thermal actuation was employed to achieve nanometer displacements and differential capacitance to measure load with nN resolution[34–36] (see Figure 2b). Other implementations consisted of in–situ electrostatic force actuators and three plate capacitive displacement sensing technologies initially developed for nanoindentation applications. In the case of in situ nanoindentation, one direction of particular interest was the study of plasticity in metals using in situ TEM nanoindentaion.[37,38] Through the direct visualization of dislocation dynamics in metallic structures these studies demonstrated nanoscale mechanical phenomena such as dislocation starvation[38] and grain boundary strengthening.[37] A detailed account of progress utilizing the above mentioned techniques has been previously given by Legros et al.[33] Although in situ nanoindentation has shed a great deal of light onto nanomechanical size effects, the interpretation of indentation testing is indirect compared to uniaxial testing methods and is not suitable for characterizing 1D nanostructures such as CNTs. In addition, traditional in situ TEM straining holders do not provide the force sensing capabilities required to fully characterize their mechanical behavior.

The challenge of conducting uniaxial mechanical testing of nanostructures in situ TEM with simultaneous load sensing has been addressed by several approaches, including atomic force microscopy (AFM) and micro-electro-mechanical systems (MEMS). Because of the advantages in using MEMS platforms for in situ TEM, our discussion will first be focused on MEMS based testing technologies. AFM techniques are also reviewed in the following section due to their application to nanomaterials despite their indirect nature and the need for models to extract properties. in situ uniaxial TEM MEMS testing requires addressing many challenges including specimen handling and loading, force sensing, and displacement or strain sensing. Prior to testing, nanometer scale specimens must be attached to the MEMS testing device. One common method is performed via a combination of nanomanipulation and bonding techniques utilizing piezoactuation and special glues or electron induced deposition[12,18,40] in situ optical or scanning electron microscopes. Loading of the specimen can be achieved by either piezo,[34] thermal,[12,40,41] or electrostatic actuation.[36,42–44] Force measurements are typically achieved by calibrated electrostatic comb drives[45] in force-controlled experiments, and deflection measurements of a force sensor beam with calibrated stiffness in displacement-controlled experiments, either through direct displacement imaging[46] or via capacitive sensing.[41] Finally, specimen displacement is determined by direct TEM imaging while atomic level strain can be measured from selected area electron diffraction (SAED) of the specimen,[40] a technique which exploits the atomic scale spatial resolution achievable in TEM (see Figure 2b). For a more detailed review of in situ MEMS based mechanical testing see the following review articles.[34,47]

2.2. Measuring Ultralow Forces: AFM Methods

One of the most fundamental requirements towards understanding the mechanical behavior of carbon-based materials at atomic level and micrometer scales, as discussed above, is high force resolution measurement. This requirement has been addressed by quantitative AFM, which allows force measurements in the nano and pico Newton regime. This capability has become one of the most widely applied mechanical testing techniques for nano structures in general, and has allowed mechanical characterization of individual carbon nano structures such as CNTs, graphene and graphene oxide sheets. In particular, AFM has been applied in a variety of implementations including membrane deflection,[13,48] as an extension of the membrane deflection experiments first developed in the study of elasticity and size-scale plasticity in sub-micron thin films,[49–51] in frictional[52,53] studies of graphene and graphene oxide as well as tensile[11,23,54] and bending studies[55] of CNTs and CNT bundles. In the case of graphene, AFM based membrane deflection was essential in confirming the extraordinary in plane strength (~100 GPa) and modulus (~1 TPa) of single layer sheets, which had been previously predicted by QM simulations (see **Figure 3**).[13] This experimental demonstration

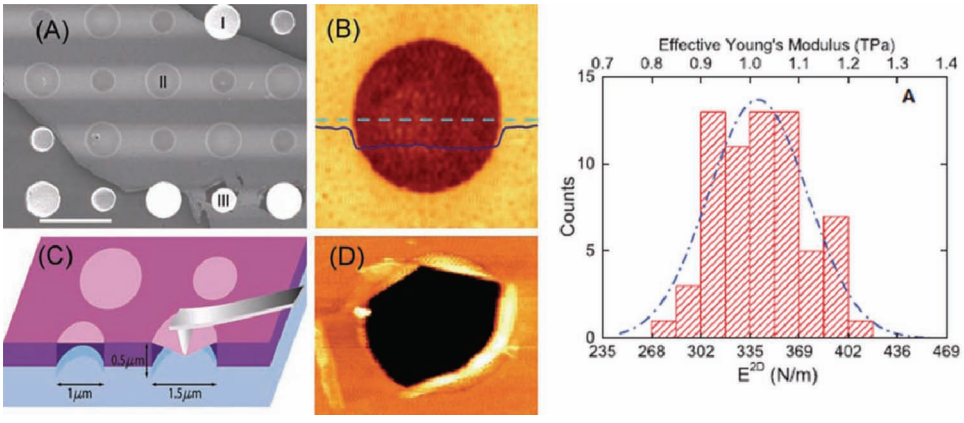

Figure 3. AFM indentation of suspended graphene sheets. (A-B) SEM and AFM images of a suspended graphene sheet. (C) Schematic representation of a AFM indentation experiment of a graphene sheet. (D) AFM image of a fractured graphene membrane. (Right) Histogram of the experimentally measured elastic modulus of graphene sheets revealing stiffness of ~1 TPa. Reprinted with permission from AAAS.[13]

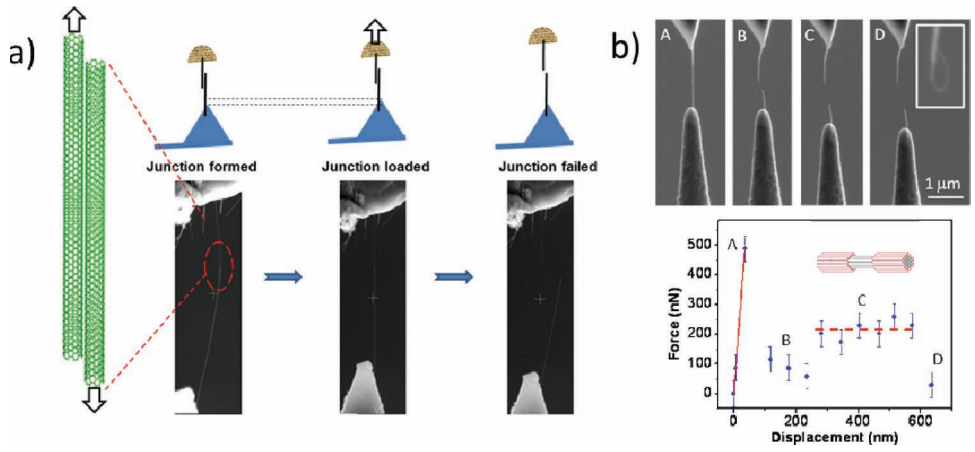

Figure 4. In situ SEM shear testing of CNT interfaces. (a) SEM images and schematics of the formation, shear testing, and failure of a junction of two MWNTs using a Si cantilever load sensor (Copyright 2012,[17] American Chemical Society). (b) SEM images and force displacement curve measured for the pullout of inner DWNTs from a DWNT bundle. Reprinted with permission,[62] Copyright (2012) American Chemical Society.

helped to spur the incorporation of graphene in hierarchical composite materials as nature's strongest and stiffest building block.

The unique force sensitivity of AFM relies on high resolution deflection sensing of a micro fabricated cantilever beam engineered to have well defined spring constants. In AFM the deflection sensing is commonly achieved via an optical laser beam deflection scheme but other techniques, such as piezo resistive detection, have also been applied. For a detailed description of both the modes of operation, as well as quantitative analysis of force measurements using AFM, the reader is referred to the following reference.[56]

2.3. Investigating Shear Interactions: in situ SEM/AFM Methods

Despite the remarkable mechanical properties of CNTs and graphene, the strengths and stiffnesses of their nanocomposites films and fibers are only a small fraction of the corresponding intrinsic properties, pointing to the inefficient load transfer between neighboring CNTs and graphene sheets. Moreover, due to the weak interactions between shells of, for example as produced MWNTs, only the outmost shell will participate in the load transfer, substantially reducing the effective strength and modulus of MWNTs. Therefore, a key element to the design of CNT and graphene based nanocomposites with high mechanical properties is to better understand and engineer the shear interactions between adjacent CNTs and graphene sheets, and shells of MWNTs.

As discussed in Section 2.1. the first experimental evidence of the sliding of the inners shells of MWNTs inside outer shells was revealed through electron microscopy visualization.[28] While these early experiments pointed to a nearly wear free shear interactions between adjacent shells of MWNTs, they did not allow the quantification of forces involved. To achieve this, in situ SEM experiments, which utilized an AFM cantilever as the load sensor with the direct visualization of electron microscopy, were developed by Yu et al.[57] Their experiments included the loading of the outer shell of MWNTs in tension, followed by its rupture and the controlled pull-out of the inner shells in a so-called sword-in-sheath failure. Due to the point-to-point resolution of the SEM, correlation between the number of failed shells and measured force was not possible. This was first accomplished by Espinosa and co-workers using MEMS technology in situ TEM.[12] In their work, the peak load and post failure load displacement curve was measured and correlated to the failure of a single CNT shell in a MWNT. Furthermore, the modulus and strength predicted by QM for a single CNT shell was achieved, for the first time, on pristine arc-discharge CNTs.

Shear force measurement between CNTs has also been obtained by incorporating AFM.[58,59] Using an AFM, Kaplan-Ashiri et al. investigated, both experimentally and theoretically, the stiffness of inter layer shear sliding of MWNTs by loading individual MWNTs in three point bending, causing small shear strains between the shells of MWNTs.[58] Another type of AFM based study of the shear interactions between CNTs was performed by mounting a MWNT on the AFM cantilever tip and scanning across a suspended single-wall carbon nanotube (SWNT) in tapping mode.[59] The variations of the AFM cantilever vibration parameters were used to estimate the frictional force and the shear strength of the contact between the two tubes.

Recently, experimental schemes coupled with theoretical models and simulations have been employed to investigate the shear interactions, in a different level of the hierarchy of CNT materials, between shells of contacting CNTs and their bundles, aiming at developing a fundamental understanding of the effect of surface functionalization and CNT surface quality on the CNT-CNT interactions[17,60,61] (see **Figure 4**).

In addition to nanoscale experiments aimed at investigating the interactions between graphitic shells in MWNTs, macroscale experiments have also been devised and implemented to indirectly measure the shear interactions between MWNTs.[63,64] These experiments typically have a higher throughput

compared to nanoscale experiments presented earlier in this section, mainly due to the size of the sample, which facilitate its preparation, and the higher forces involved. However, the larger scale experiments can only quantify the average response of the MWNT sliding, without being able to elucidate the details of their atomic scale sliding.

2.4. Collective and Local Behavior: Micromechanical Testing Methods

Due to their remarkable mechanical properties, since their discovery, CNTs have been considered as one of the promising fillers for nanocomposites, adding strength and stiffness to different matrices. In general, based on relative mass/volume CNT content, CNT based nanocomposites can be divided into two groups: nanocomposites with low and high CNT ratio. The demarcation line between the low and high CNT content can be considered to be the percolation threshold of CNT concentration, above which a continuous network of CNTs will develop in the composite facilitating the transfer of mechanical load, electric charges and heat. The latter type of CNT nanocomposites (containing high concentration of CNT) has become an active field of research especially in the last decade, and is the main focus of this section. More general reviews of CNT composites, which focus on low CNT ratio composites, and their processing and mechanical properties, can be found elsewhere.[65,66] As pointed out in the previous section, by enhancing the shear interactions between CNTs *in high CNT* content nanocomposites, the remarkable mechanical properties of CNTs at the nanoscale should be achieved at the macroscale. In addition, higher contents of CNTs in nanocomposites can enhance both their electrical properties and thermal stability. Several methods have been commonly used to investigate the mechanical behavior of CNT based composites, including dynamic mechanical analysis (DMA), micro tension tests on CNT based composites and yarns, and in situ mechanical characterizations inside analytical chambers such as an SEM or Raman spectrometer.

DMA is typically used to investigate the viscoelastic response of CNT-polymer composites, and it can be used to investigate the interactions between CNTs and polymer chains.[67–71] In DMA, a sinusoidal stress field is applied to the sample and the strain response is monitored. From the analysis of the DMA experiments, the dynamic moduli of the CNT-polymer system with two major components are extracted: the storage modulus and the loss modulus, both functions of the strain oscillation frequency. The former modulus is a measure of the mechanical energy stored in the system, and the latter represents the energy loss in the system, mostly in the form of heat. DMA experiments on CNT composites are typically carried out in a temperature sweep mode to reveal information about the glass transition temperature (T_g) of the system and its variations with CNT-polymer interactions. Generally, the dependence of T_g on CNT content contains information about the nature of interactions between CNTs and the polymer matrix.

Tension tests have also been widely used to measure the mechanical behavior of CNT composites, (see **Figure 5**a–d). Unlike DMA experiments, which reveal only the viscoelastic mechanical properties of the composites, in tension tests other material properties such as strength and energy to failure have also been reported.[29,67,72–75] These parameters are all of significant interest to the design of high performance composites and yarns.[23] In addition, the statistical analysis of fracture parameters such as toughness, strength and ductility can be instrumental in obtaining an average distribution of defects in the samples.[21] The shape of the stress-strain curves, obtained in tension tests, provides evidence about the deformation mechanisms in CNT composites and the ensemble behavior of the CNT-polymer chain interactions.[72] Tension tests on CNT composites carried out in situ analytical chambers such as SEM and Raman can also be used to reveal the microscopic mechanisms of deformation of CNT composites. For example, Espinosa and co-workers, investigated the effect of lateral contraction and twisting of CNT yarns inside SEM chambers.[23] Moreover, mechanical testing in situ Raman spectroctrometer has been used to assess the local strain distribution in mechanically loaded CNT composites, as shown in Figure 5e,f.[29,76] In Raman spectroscopy, the sample is excited by a monochromatic light source, and the inelastic scattering of light is collected. The shift in the frequency of the scattered light, compared to that of the incident light is a characteristic of the modes of vibration of the sample and atomic spacing. For instance, in the Raman spectrum of CNTs, the so-called radial breathing mode (RBM) peaks, the graphite (G) peak and the disorder (D) peak are among the most commonly studied signatures. The RBM modes (scattering shift of <300 cm^{-1}) reflect the vibration of carbon atoms of CNTs in the radial direction, and are characteristic of the diameter of CNTs. The G peak (scattering shift at ~1600 cm^{-1}) results from the in-plane vibration of carbon-carbon bonds, and reflects the graphitic nature of CNTs, while the D peak (scattering shift at ~1300 cm^{-1}) is the defect-induced peak.[77,78] In in situ Raman experiments, straining of CNTs will result in the change of the carbon-carbon interaction energy and the frequencies of their different modes of vibration, inducing a change in the Raman signal shifts. This shift in the Raman signal can be collected, for instance during a tension test experiment on a CNT composite, to estimate the average strain in CNTs at different loading conditions.[29,76]

Another type of experiment used to investigate the mechanical properties of CNT based materials is nanoindentation.[80–85] In this type of experiment, an indenter is pushed against the sample surface, and the mechanical interactions between the two are extracted and used to calculate the sample modulus and hardness at the location of the indentation. Moreover, by modifying the sample boundary conditions and utilizing proper nanoindenter tip geometry, a nanoindentation setup can be used to perform bending and compression experiments on composites.[30,82] In a nanoindentation experiment, the modulus is calculated by measuring the unloading stiffness of the nanoindenter, and hardness is measured as the ratio of the maximum load to the residual indentation area.[86] The main advantage of nanoindentation over other mechanical characterization methods is that it does not require extensive sample preparation, which becomes specifically beneficial for nanoscale samples such as electrospun nanofibers containing CNTs.[84] Moreover, it allows for the measurement of local mechanical properties of the samples. In the case of composites with nanofiller reinforcement, such as CNT based composites, together

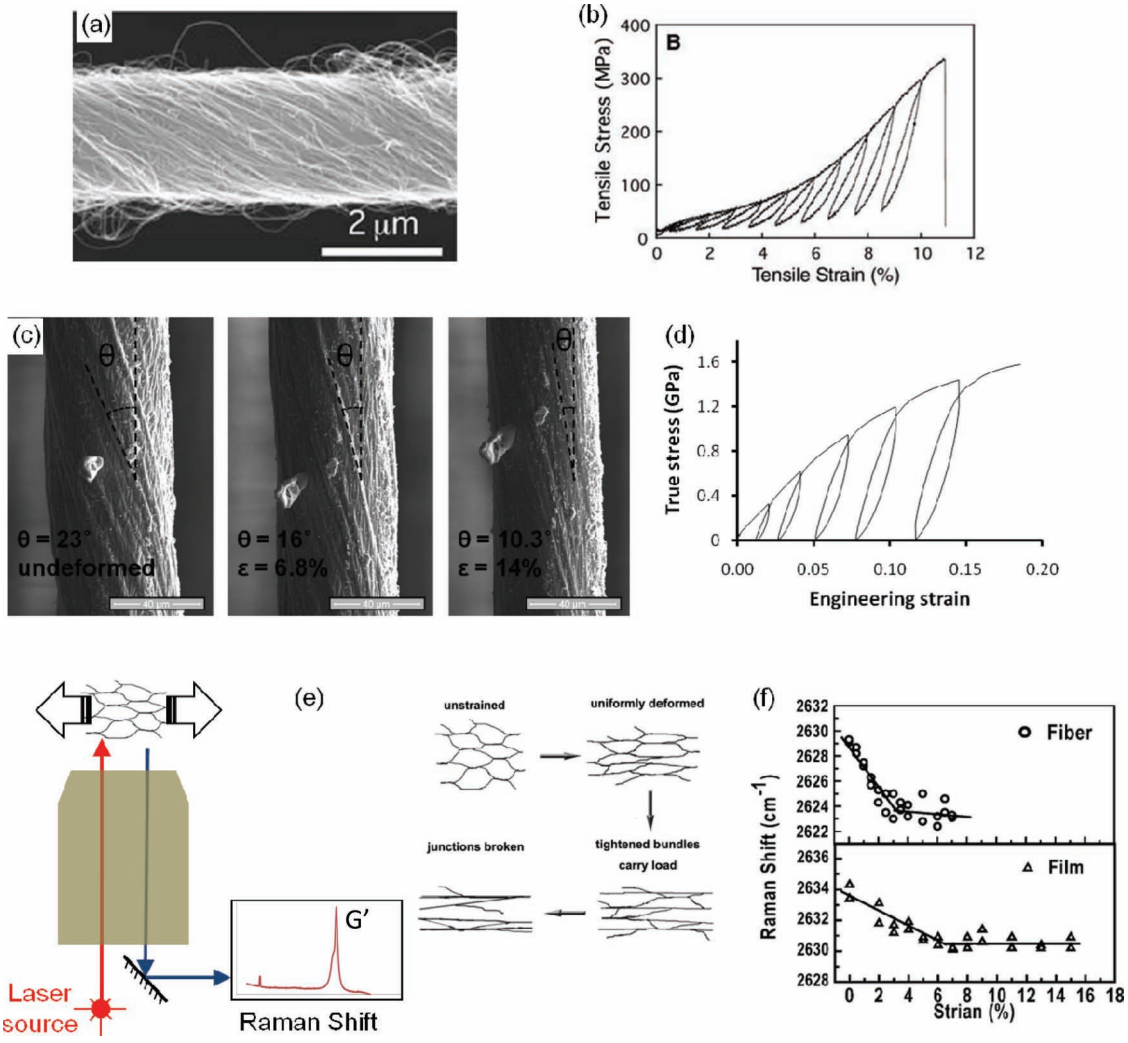

Figure 5. Micromechanical testing methods applied to CNT yarns. (a) SEM image of the CNT yarns spun from a forest of CNTs and (b) its mechanical behavior measured in tension, Reprinted with permission from AAAS.[79] (c) Three snapshots of the tension test on a CNT yarn, tested in situ SEM. The Poisson ratio of the yarns are ~1 as measured as the ratio of the axial strain to the relative change in diameter of the yarn. (d) The mechanical behavior of the yarn shown in (c) Adapted with permission[23] Copyright 2010, American Chemical Society. (e) Schematics of the in situ Raman tension tests on CNT yarns fabricated from forests of CNTs, and the corresponding changes in the location of the G′ peak as a function of strain (Adapted from [29]).

with rule of mixture estimates of elastic moduli, nanoindentation becomes an enabling tool for correlating CNT dispersion inhomogeneities with mechanical properties.[85] The main disadvantage of nanoindentation is that due to its indirect nature, a model for the mechanical behavior of the sample and tip is required to extract the samples materials properties.

3. Hierarchical Carbon-Based Materials

In the following we will review progress in the development and understanding of hierarchical carbon-based materials, which has been achieved through the application of the multiscale experimental techniques discussed in the previous section. In particular, the focus will be on materials that utilize a high density of CNTs, graphene, or graphene oxide as building blocks. Such materials, which are based primarily on constituents with a high level of order, are envisioned to allow for optimal properties similar to those found in nature. A focus on CNTs and graphene is motivated by their extraordinary intrinsic mechanical properties, which have been recently confirmed.[12,13] For a detailed review on the intrinsic mechanical properties of individual CNTs and graphene sheets the reader is referred the following review article.[87]

3.1. Weak Shear Interactions between Adjacent Graphitic Layers

One consequence of developing hierarchical materials with a high density of highly ordered graphitic layers (graphene sheets and CNT shells) is the corresponding high density of direct interactions between adjacent graphitic layers. As discussed

previously, this poses one of the greatest challenges to scaling up the exceptional mechanical properties of CNTs and graphene to macroscopic materials, as these interfaces tend to have inherently weak interactions dominated by van der Walls (vdW) forces. Examples of these interfaces include shell-shell interactions in MWNTs, tube-tube interactions in close-packed CNT bundles, and sheet-sheet interactions in few layer graphene. These weak interfacial interactions lead to low strength shear transfer between adjacent layers, which significantly limits the effective mechanical performance of the macroscopic constituents. As pointed out in Section 2.3., the investigation of binding energy and load transfer between such graphitic layers can provide us with deeper insight into the mechanical behavior of carbon-based composites, and potentially opens new horizons in designing CNT and graphene based composites with enhanced mechanical performance.

One of the first direct demonstrations of easy shear between individual adjacent graphitic layers was through in situ TEM axial stretching of MWNTs.[28] Cumings and Zettl visualized the pull out of the inner shells of a MWNT from the outmost shell of MWNTs, in situ TEM, by welding a probe to the inner shells and pulling the inner shells out. Figure 2a shows the inner shells of a MWNT being pulled out of an outer tube of shells in a reversible process. Without measuring the pull out force experimentally, they estimated the vdW interlayer force to be in the order of 9 nN corresponding to 2.3×10^{-14} N per atom. They demonstrated that the pulled out inner shells tend to be pulled back in, due to the vdW interactions between the inner and outer shells, without any detectable damage to the atomic structure of CNTs, pointing to nearly perfect sliding surfaces with minimal wear. Subsequent pullout studies, which utilized an AFM force sensor in situ TEM, estimated that the interlayer shear was dominated by van der Walls interactions.[88] In this study the interlayer shear strength was estimated to be < 0.05 MPa, with an interlayer cohesion energy of 33 meV/atom, which was in good agreement with estimates determined from an energy analysis of collapsed MWNTs.[89]

The interactions between shells of a MWNT was also quantified by Yu et al.[57] They used an AFM cantilever as the load sensor mounted on a manipulator inside an SEM. One end of a MWNT was attached to the AFM cantilever tip, while the other end was attached to a substrate, both by carbon deposition. In the experiments, the outer shell of a MWNT was pulled in tension. First the outer shell of the MWNT ruptured, which was followed by controlled pull out of the inner shells. The pull out force measured by Yu et al. was described as being composed of two components: the shear interaction between shells, which scales with the overlap (embedded) length; and a second interaction, induced for instance by the capillary effect and the interactions by dangling bonds at the two ends of the shells, which scales only with the circumference of the inner tube. The static shear strength was estimated to be 0.08–0.3 MPa, and the combined capillary and edge effect force was measured to be 80–150 nN, dominating the experimentally observed forces. In this study, it was assumed that the shear transfer takes places along the whole contact length between the inner and outer shells. Therefore, the active overlap length could be overestimated, and the reported shear strength represents a lower bound. However, given the finite stiffness of the CNTs, the shear forces could be distributed over a shorter length, leaving the rest of the CNTs traction free. This could in part explain the wide range of measured shear strength between CNT shells presented in.[57] While such nanoscale experiments can quantitatively capture shear sliding between layers of MWNTs, due to the limited resolution of SEM in measuring the interlayer sliding, they are not capable of capturing the interlayer sliding shear modulus.

Kaplan-Ashiri et al. investigated, both experimentally and theoretically, the stiffness of inter layer shear sliding of MWNTs, by loading individual MWNTs in bending using an AFM to achieve sub-nanometer deflection resolution.[58] Their theoretical analysis, using the density function based tight binding (DFTB) method, pointed to an interlayer shear modulus of about 2 GPa. The relatively low value of the interlayer shear modulus compared to axial modulus of CNTs (the ratio of shear modulus to axial modulus of CNTs is ~0.02 compared to a value of 0.3 for an isotropic material) resulted in considerable shear sliding between shells of the MWNTs in the AFM bending experiment, such that as much as 25% of the lateral deflection of CNTs was due to elastic shear deformation. For comparison, the shear deformations would contribute to less than 1% of the total lateral deformation of an isotropic material with similar dimensions. Locascio *et al.* applied an in situ TEM method to measure the shear sliding between inner and outer shells of a MWNT.[39] They measured an average post failure force of 35 nN required to pullout the 11 inner shells of a 14 nm diameter MWNT with respect to the outer shell (see Figure 2b).

CNT bundles have also been shown to exhibit weak interaction between adjacent outer CNT shells within close-packed bundles. In situ SEM tensile experiments conducted on single (SWNT) and double walled (DWNT) nanotubes revealed a similar sword-in-sheath failure mechanism in which inner CNTs within bundles pulled out with respect to an outer shell of CNTs.[23,54] Yang et al. experimentally investigated the friction between SWNTs by loading a SWNT bundle in tension.[63] Their SWNT bundles were relatively long (~3 mm) and were grown in a CVD reactor. During the tensile loading, they monitored both the elastic behavior and the inelastic behavior of the yarns due to SWNTs sliding on each other. They estimated the cohesive energy per unit area of the SWNTs to be in the range of 0.1 Jm^{-2} to 0.6 Jm^{-2}, by normalizing the friction energy (dissipated during the plastic deformation) by the change in the contact area between the bundles. While this method can be used to obtain an average value for the cohesive energy between SWNTs studies, it suffers from uncertainties in the estimation of the edge effect and the true contact area between SWNTs. More recently a novel method of in situ SEM peeling between two SWNT bundles was used to measure an adhesion energy of 0.12–0.16 nJ/m;[90] however, the width of the contact between the two bundles was not reported, therefore the cohesion energy per unit area is unknown, making comparison with other studies difficult. The nature of shear interactions within DWNT bundles has also been recently investigated via an experimental-computational approach which compared in situ SEM pullout tests to MM and DFT simulations.[62] In this study Filleter et al. measured a normalized pullout force of 1.7 +/–1.0 nN/CNT-CNT interaction for sliding of a smaller inner bundle of DWNTs out of a larger outer shell of DWNTs (see Figure 4b). Through comparison with MM and DFT simulations

of sliding between adjacent CNTs in bundles it was identified that factors contributing to the pullout force included the creation of new CNT surfaces, carbonyl functional groups terminating the free ends, corrugation of the CNT-CNT interaction, and polygonilization of the CNTs in the bundle. In addition a top down analysis of the experimental results revealed that greater than one half of the pullout force was due to dissipative forces. This finding of behavior at the CNT bundle level significantly differs from the behavior of pullout in individual MWNTs for which dissipation is found to be negligible.[28]

Bhushan et al. investigated the interactions between an individual SWNT and MWNTs in ambient conditions using an AFM.[59] The former was mounted over a trench on a substrate, while the latter was mounted at the tip of an AFM cantilever. The cantilever was scanned over the trench in tapping mode to induce contact between the SWNT and MWNTs. The maximum deflection of the cantilever as the MWNT was pulled away from the SWNT was used to estimate the work of adhesion between the two tubes as 0.03 Jm^{-2}. This value is significantly lower than previous measurements of the graphite surface energy,[91] potentially due to the uncertainties in the contact area between the two tubes. Therefore, it should be considered as a lower bound for the work of adhesion in graphite in ambient conditions. In addition, the attenuation of the amplitude of vibration of the cantilever, upon the formation of contact between two CNTs, was used to estimate the power loss due to friction, from which the friction force and the shear strength of the contact between the two tubes was estimated. The shear strength was estimated to be ~4 MPa, which is higher than that measured in vacuum,[57] most likely due to the presence of thin layers of water molecules strengthening the junctions between the two tubes in ambient conditions.

Peeling experiments have also been used to investigate the interactions between graphitic surfaces. Ishakawa used a self-detective microcantilever inside an SEM chamber to measure the interactions between a MWNT and cleaved graphitic surfaces in pure peeling mode (mode I) with negligible net shear stress component on the interface.[92] They observed discrete jumps in the adhesive force with the peak values in the range of a few tens of Nanonewtons, corresponding to adhesive energies of as high as 78 keV, with the number of discontinuous jumps decreasing as the length of the CNTs decreased, due to the enhanced bending stiffness of the MWNTs.

Wei et al., developed a continuum based shear-lag model which successfully predicted the saturation regime in the shear force as a function of overlap length for SEM experiments of shear between MWNTs, the details of which are shown in Figure 4a.[17] In this study the data from shear experiments performed on un-functionalized MWNTs fell into the region in between two theoretical curves with shear strengths of 30 and 60 MPa for arm-chair and zig-zag tubes, respectively. This suggested that the shear between two MWCNTs is dependent on chirality, which was also verified by atomistic calculations. Furthermore, through their model they demonstrated that CNT alignment, although required, is not the sufficient condition for optimal mechanical performance of CNT based yarns. Rather, the average overlap lengths between CNTs needs to be chosen properly, based on the mechanical properties of the constituents and the shear interactions between CNTs, to achieve highest mechanical performance, such as the highest elastic energy density and full utilization of the CNT strength. Likewise, to achieve ductility and associated high failure energies, spreading of the sliding and delay of deformation localization is needed.[9] It is however to be noted that the complexities and limitations related to fabrication of CNT yarns with a prescribed architecture (characterized by parameters such as overlap length and alignment) remains to be addressed. Similar experimental-analytical approaches can be implemented to realize the role of CNT surface functional groups and crosslinking chemistries on the enhancement of CNT interface interactions.

In addition to microscopic studies of shear within CNTs and bundles, weak interlayer binding and shear between adjacent graphene layers has also been extensively studied indirectly through a variety of techniques including macroscopic friction testing of graphite.[93] It is generally accepted that graphite acts as a good solid lubricant due to shearing of adjacent graphitic planes. More recently nanometer scale friction measurements on graphite and graphene have confirmed ultralow frictional properties.[52,94] In addition several experimental techniques, including heat of wetting experiments[95] and molecule desorption studies,[96] have measured the cohesion energy of graphite to be 0.26–0.37 J/m^2, similar to the reported measurements on CNTs and CNT bundles. A summary of both the shear strengths and cohesion energies measured for the variety of interfacial systems discussed in this section is found in **Table 2**.

3.2. Crosslinking Adjacent Graphitic Layers

One approach to address the limitation of weak interlayer shear between graphitic layers, as discussed in the previous section, is the introduction of crosslinking bonds between adjacent sheets. This approach inherently requires modifications to the in-plane sp^2 bonding within the graphitic sheet. In the case of CNTs, one method to achieve this is via high energy electron irradiation at energies above the knock on requirement to displace or remove carbon atoms and create covalent crosslinking defects, whereas in the case of graphene, chemical surface modifications have been applied to create graphene oxide sheets in which functional surface groups are utilized to enhance interlayer linking.

Table 2. Experimentally determined interfacial properties of graphitic materials.

Material interface	Shear strength [MPa]	Cohesion energy [Jm^{-2}]	Environment	Ref
MWNT shells	0.05	0.198	TEM/high vacuum	[88]
MWNT shells	0.08–0.3	-	SEM/high vacuum	[57]
Bundled SWNTs	-	0.1–0.6	Air	[63]
SWNT/MWNT	4	0.03	Air	[59]
Collapsed MWNT shells	-	0.21	TEM/High vacuum	[89]
Graphite layers	-	0.26	Air	[95]
Graphite/ aromatics	-	0.37	Air	[97]

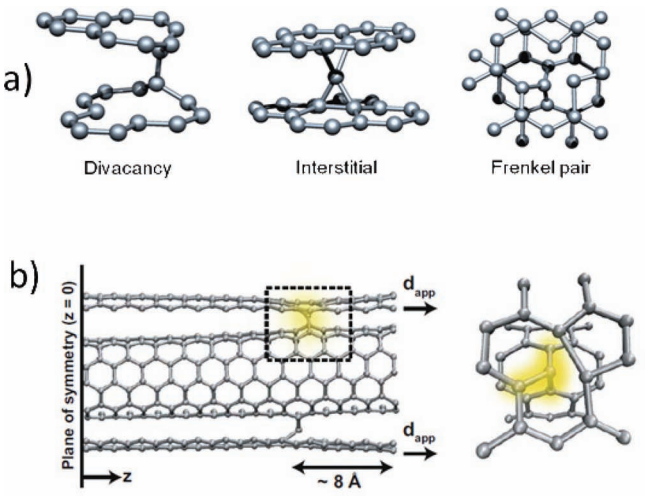

Figure 6. (a) Irradiation induced defects predicted to form between adjacent atomic layers in graphite. Adapted with permission from Macmillan Publishers Ltd: Nature,[99] copyright 2003. (b) Molecular mechanics simulation of load transfer for Frenkel pair defects between the outer and inner shells of a double-walled carbon nanotube Adapted with permission,[39] copyright 2009, SEM.

Irradiation by high energy particles, such as ions, electrons, or neutrons, to induce modifications to carbon nanostructures has been predicted and demonstrated to result in the creation of vacancy and interstitial defects that can bridge adjacent atomic layers.[98,99] This has proven to be a unique method to greatly enhance the effective properties of both MWNTs and CNT bundles. Quantum mechanics calculations have demonstrated that irradiation leads to the formation of divacancy, interstitial, and Frenkel pair defects (see **Figure 6**a) resulting in covalent bonds being formed between adjacent graphitic sheets.[99] Molecular mechanics simulations have shown that only a low density (~0.2–0.4 defects/Å) of such defects is required to approach theoretical limits of load transfer between adjacent graphitic sheets, such as inner and outer shells in DWNTs (See Figure 6b).[12,39] This approach towards achieving efficient load transfer facilitated by crosslinking defects has been applied to address load transfer at multiple lengths scales within CNT based materials. In the majority of high density CNT based materials, the first two hierarchical length scales are shell-shell interactions within individual MWNTs and tube–tube interactions between adjacent outer shells, both of which have been demonstrated to be successfully crosslinked by irradiation.

At the first hierarchical level, Peng et al. demonstrated the effects of electron irradiation crosslinking through in situ TEM tensile testing experiments conducted on irradiated MWNTs.[12] In these studies high resolution TEM imaging revealed that in the absence of irradiation only the outer shell of the MWNT carried an appreciable load until failure after which it slid with respect to the inner shell by the previously documented sword-in-sheath failure mechanism. At higher irradiation levels MWNTs were found to fail across multiple shells as load transfer to inner shells was increased due to crosslinks. Analysis of the true stress acting on the shells carrying load revealed that at low levels of irradiation the outer few CNT shells had a remarkable failure stress and modulus of ~100 GPa and ~1 TPa, respectively, whereas increased irradiation led to a reduction in true strength and modulus to 35 GPa and 590 GPa, respectively.[12] This demonstrates the inherent tradeoff between enhancing the effective mechanical properties of the MWNT while at the same time reducing the intrinsic mechanical properties of individual CNT shells through the creation of defects.

At the tube-tube level Kis et al. applied an AFM based deflection method to investigate the effects of electron irradiation induced crosslinking on enhancing the bending modulus of SWNT bundles (see **Figure 7**f-g).[55] Here it was demonstrated that low doses (~5×10^{20} e/cm^2) of electron irradiation yielded an increase in the effective bending modulus up to ~750 GPa.[55] Again, higher irradiation doses significantly reduced the modulus, in this case to as low as ~100 GPa (at doses > 40×10^{20} e/cm^2). The AFM based method, however, did not allow for a determination of the strength of the irradiated SWNT bundles. More recently, Filleter et al. conducted in situ TEM studies on DWNT bundles exposed to high energy electron irradiation.[18] In this case both levels of hierarchy, inter tube shell-shell interactions as well as inter bundle tube-tube interactions, are present and crosslinked via irradiation.[18] Here it was found that both the effective strength and stiffness of the DWNT bundles was increased by irradiation up to 17 GPa and 693 GPa respectively (see Figure 7a–e). HRTEM images of the DWNT bundles revealed that in the case of minimally irradiated bundles (0.5×10^{20} e/cm^2) the outer tubes within the bundles failed during the tensile test and slid with respect to the inner bundle of DWNTs, akin to the sword-in-sheath failure observed for MWNT shells. However, at optimal irradiation doses (~$9–11 \times 10^{20}$ e/cm^2) the bundles were found to fail across the entire cross section of shells and tubes confirming effective load transfer to the entire inner core of material. The potential benefits of irradiation induced crosslinking have also been investigated via MD simulations of CNT bundles. Cornwell et al. recently conducted simulations of SWNTs crosslinked by interstitial carbon atoms which predicted significantly increased load transfer leading to strengths of up to 60 GPa for SWNT bundles with optimal crosslinking density and overlap geometry.[100] Although all of these studies have demonstrated that irradiation induced crosslinking is effective at improving load transfer within CNTs and bundles, they have also identified that there is a limit in the achievable mechanical properties, as the complexity of the material is increased due to the inherent introduction of structural defects into the material.

Another approach which has been implemented recently to develop high performance CNT yarns and to enhance the shear interactions between CNTs is the *in situ* CVD functionalization of tubes (DWNT bundles).[23] Unlike conventional methods for the functionalization of CNTs, this method which is based on the development of polymer radicals inside the CVD reactor, together with the formation of DWNT bundles with very low defect density, allows for the covalent functionalization of DWNT bundles at the existing defect sites with active polymer species such as substituted acrylic acid groups, therefore, maintaining the integrity of the structure of the bundles. Nanoscale experiments on the effect of in situ CVD functionalization of the tubes on the shear interactions between DWNTs together

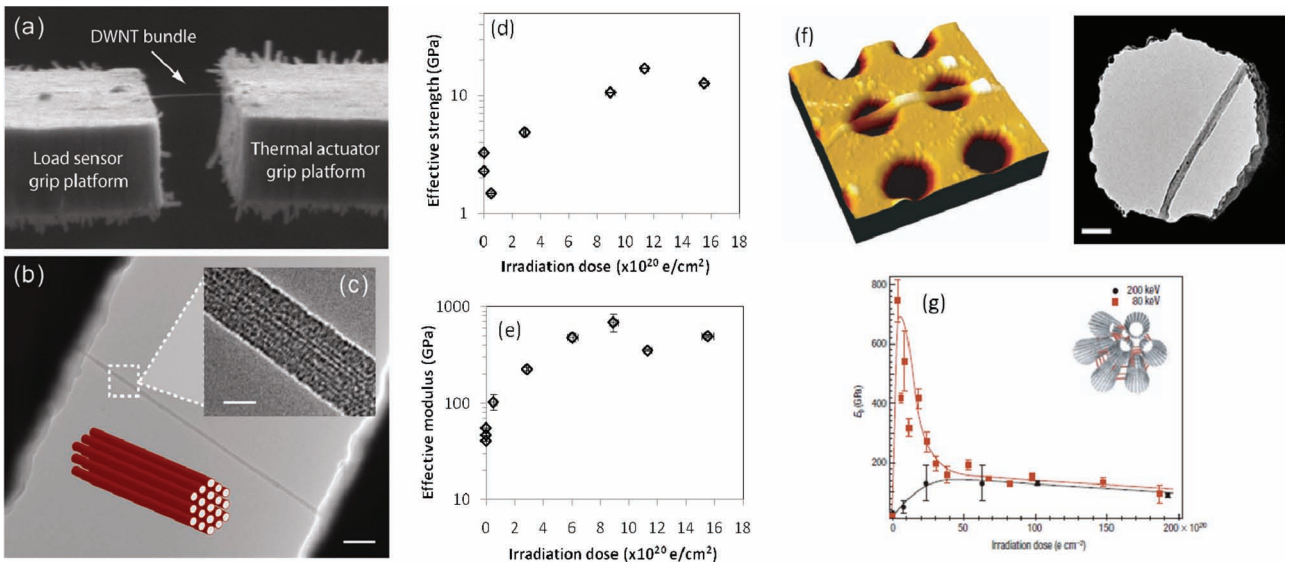

Figure 7. Irradiation induced covalent crosslinking enhancements in DWNT and SWNT bundles. (a–c) in situ TEM tensile testing of DWNT bundles. (d-c) Enhancements in effective strength and modulus for DWNT bundles as a function of irradiation dose (Adapted from [18]). (f) AFM based deflection experiments of SWNT bundles. (g) Enhancements in effective bending modulus for SWNT bundles as a function of irradiation dose.[55] Adapted with permission from Macmillan Publishers Ltd: Nature Materials,[55] copyright 2004.

with the multiscale simulations of the shear experiments have pointed to shear strengths of as high as 300 MPa, mostly due to the interlocking mechanisms between the polymer chains of the shearing bundles and the high degree of alignment of polymer chains achieved during the process of shearing.[60] These strong interactions have led to unconventional strength and energy to failure of as high as 1.5 GPa and 100 J/g, respectively.[23] Coarse-grain molecular modeling is emerging as an attractive technique which enables studying the effects of polymer crosslinking in large CNT bundles and fibers. Through course-grain modeling Bratzel et al. have demonstrated that polymer crosslinks with optimized concentration and length can lead to increases of four-fold in strength and five-fold in toughness for crosslinked CNT bundles.[101]

In the case of graphene, a similar challenge exists in improving load transfer from one graphene sheet to the next. At the core of the challenge is the lack of reactive chemical handles on the basal planes. In addition to electron irradiation induced crosslinking, another attractive method to address this limitation, which has been applied to graphene, is the oxidation of graphite to produce graphene oxide (GO) sheets, which bear oxygen functional groups on their basal planes and edges. These functional groups then act as chemical crosslinking sites between adjacent sheets. Despite the similarities between the atomic structures of CNTs and graphene, their responses to functionalization processes may be very different. On one hand, graphene will likely start to react with functional groups at the edges and the defects where dangling bonds are present. On the other hand, the surface curvature of CNTs and the associated bending energy stored in C-C bonds facilitates the chemical reaction of C atoms with functional groups. In the case of GO, similar limitations on the mechanical properties exist to those demonstrated for irradiation induced crosslinking of CNTs: the oxidation process inherently leads to the formation of voids in the graphene lattice, which reduces the strength and stiffness. AFM based experiments, similar to those used to demonstrate the exceptional strength and stiffness of pristine graphene sheets,[13] have demonstrated that by oxidizing graphene to create GO the elastic modulus is reduced from ~1 TPa to 208 GPa.[48] It should also be noted that further reduction of GO, which attempts to return the structure to a pristine state, has yielded a material with a stiffness of 250 GPa, therefore not recovering the exceptional mechanical properties of pristine graphene.[102] Although no quantitative study of the strength of GO has been conducted to date, the reduction in stiffness and the observed defect structures observed via HRTEM imaging of GO[103] suggests a substantial reduction in the strength of GO. If we assume a correlation between the reduction of modulus and the induced defect density in the graphitic structures, the higher reduction in modulus observed for GO as compared to irradiated CNTs would suggest strengths of less than 17–35 GPa for GO.[12,18] This is one area in which novel fabrication methods are needed to reduce both the size and density of defects in oxidized graphene sheets while maintaining enough functional groups to facilitate effective crosslinking handles. To this effect, initial studies on tuning the C/O ratio of graphene oxide are just beginning to emerge.[104]

Despite the intrinsic reductions in the mechanical properties of oxidized graphene sheets, the effective benefits of crossliking adjacent layers of GO has shown some promise towards macroscopic graphene based materials. In its un-crosslinked state, GO paper already exhibits mechanical properties superior to many technologically relevant paper materials such as bucky paper, flexible graphite, and vermiculite. However, when compared to the intrinsic behavior of graphene, it exhibits mechanical properties that are orders of magnitude lower, i.e., a modulus of ~32 GPa

and a strength of ~80 MPa.[27] These reductions are mainly influenced by characteristics of the hierarchical structure, such as the discontinuous layering and inherent waviness, as well as weak interlayer shear interactions. Initial chemical methods to enhance the layer-layer shear interactions have included introducing divalent ions and polyallylamine crosslinks.[105,106] While these reports have shown some improvements in the macroscopic mechanical properties of the paper materials, the enhancements have been only minor and the underlying mechanisms remain to be studied via experiments and simulations at smaller length scales.

3.3. Local Mechanical Properties of CNT/Graphene Composites

One of the great challenges in developing advanced carbon-based composites is bridging an understanding between the mechanics of the nanoscale constituents and macroscopic materials. In the previous two sections, progress in understanding the mechanical behavior of CNT and graphene building blocks and how two elements (e.g., two adjacent CNTs or G/GO nanoparticles) interact was discussed. The next level of hierarchy within a carbon-based material that requires a more fundamental understanding is small networks composed of many of these building blocks. To investigate this length scale, experimental techniques are required that both probe local mechanical properties on volumes of the order of a few hundred nanometers, and measure average local behavior of many interacting nanoscale constituents. One notable example of the latter is measuring the average strain in individual CNTs in a loaded composite.

The local mechanical response of CNTs within larger networks has been investigated by utilizing mechanical testing in situ Raman spectroscopy. Given the sensitivity of the location of peaks of the Raman spectra of CNTs to the applied strain, tension tests in situ Raman spectrometry has also been used to assess the efficiency of load transfer between CNTs in a composite. In such experiments an average local strain on CNTs can be estimated as a function of the shift in Raman peaks, and compared to the global strain on the sample.[29,76] Ma et al. investigated the shifts in the G peak shape and location to identify the micromechanical mechanisms of deformation of CNT fibers and films.[29] At sufficiently low strains, they observed a downshift in the G peak, potentially due the straining of individual CNTs and the resulting weakening of C-C bonds. However, the rate of shift relative to the composite average strain was a small fraction of the value corresponding to strained individual CNTs,[107] indicating that most of the macroscale strain was due to the change of the shape of the CNT network through CNTs rotation towards the stretching direction, rather than their stretching, to accommodate the global strain. At higher strains, the location of the G peak become stationary, pointing to a change in the deformation mechanism from CNT network stretching to network rupture and stress redistribution, such that the average strain in individual CNTs remained nearly unchanged. Moreover, the straining of the samples resulted in G peak broadening, attributed to non-uniform strain in different regions of the sample.

Another type of experiment that has been applied to the investigation of the local mechanical properties of CNT/graphene based materials is nanoindentation,[80–83] which is capable of measuring material properties, such as modulus and hardness, on localized volumes confined to between tens and hundreds of nanometers. This capability of nanoindentation has been specifically useful in the assessment of the quality (uniformity) of dispersion of CNTs in CNT composites.[85] For instance, Bakshi et al. utilized the distribution in CNT dispersion (measured by image processing of the composite surfaces) together with the Halpin-Tsai relation to successfully explain the scatter observed in the composite moduli measured by nanoindentation.[85] Therefore, a reverse method in which the local modulus measurements of a composite by nanoindentation are used to quantitatively express the dispersion of CNTs in composites is imaginable.

AFM based methods have also been used to perform nanoindentation experiments on CNT composites.[84,85] The sharpness of AFM cantilever tips, in the range of few tens of nanometers, allows for the indentation of nanometer scale samples. The tilt of the AFM cantilever should either be included in the data analysis to estimate the normal indentation force from the cantilever deflection, or a tilt compensation scheme should be experimentally implemented.[108] In addition, for uncompensated experiments, given the inherent tilt of the AFM cantilevers with respect to the sample surface, pushing the AFM cantilever tip down on the sample will generate some forward motion of the tip, further complicating the data analysis. Therefore, AFM based indentations should, in general, only be carried out to induce relatively shallow indents, such that reliable loading-unloading curves can be obtained and to avoid excessive material pile-up, which can complicate the stress field.

In the application of nanoindentation to investigate the mechanical behavior of composites, care should be taken in choosing the proper type of nanoindenter tip and the boundary conditions of the sample to distinguish between different modes of sample loading, namely indentation and sample bending, and proper models should be incorporated to extract the mechanical properties of the sample.

An example of different loading modes using a nanoindentor is the work by Lee and Cui, in which they used a nanoindenter to load CNT based nanocomposite films both in indentation (collapsed samples, sitting on a substrate) and bending (a free standing film gripped on two edges) mode.[82] The geometry of the nanoindenter tip provides a helpful guideline to distinguish between the two cases: a flat tip, wider than the width of a free standing sample favors the bending experiment, while a sharp tip, with a tip radius sufficiently lower than the width of the sample, on a collapsed sample provides a stress field closer to an ideal indentation experiment.

In addition to nanoindentation and bending experiments, a nanoindenter can be used to measure the mechanical properties of CNT composites in compression, by incorporating a flat punch as the nanoindenter tip. For instance, Garcia et al. used a nanoidentor with flat punch to investigate the compressive modulus of CNT epoxy nanocomposites with CNTs oriented parallel to the loading direction.[30] A schematic of their setup is shown in **Figure 8**. They reported a substantial increase in compressive modulus of the composites from 3.7 GPa to 11.8 GPa

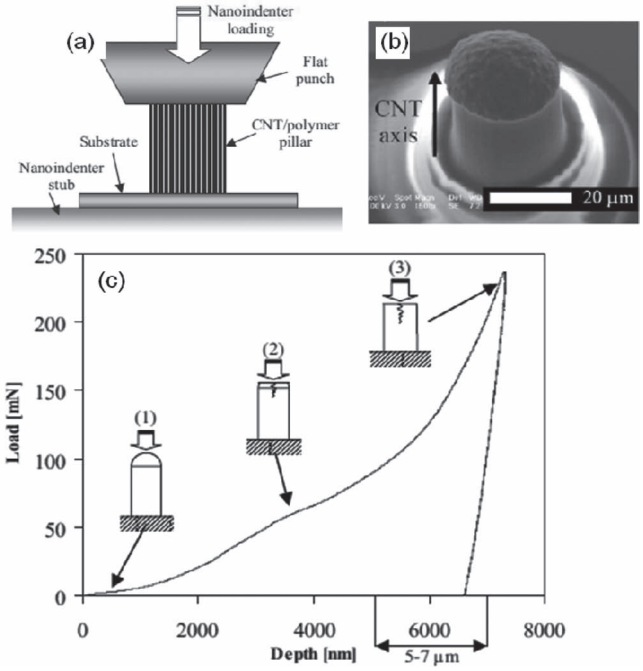

Figure 8. Schematics of (a) a nanocompression experiment on vertically aligned CNT-epoxy composites, and (b) CNT-epoxy nanopillar composite. (c) Plot of typical axial compressive force as a function of the indentation depth (Adapted from [30]).

by adding 2 volume% of CNTs. Compression tests of multilayer CNT-polymer arrays have also been conducted recently by Misra et al.[109,110] These multilayer structures were found to sustain large compressive deformations and exhibit high energy absorption as compared to synthetic materials of similar density.

3.4. High Volume Fraction CNT Fibers and Composites

One of the focuses of research in the past decade has been the development of CNT based composites and fibers with high volume fractions of CNTs. In these novel materials, unlike conventional CNT composites, due to the high concentration of CNTs, which is well above the percolation threshold, the mechanical load is transferred through a continuous network of CNTs. Therefore, the mechanical properties of the composite are substantially controlled by the average interactions between adjacent CNTs. This is in contrast to conventional composites, where the interaction between CNTs and the matrix controls the overall mechanical behavior of the composite. Several experimental techniques have been commonly used to investigate the ensemble behavior of CNT composites and fibers with high CNT concentration, such as dynamic mechanical analysis (DMA) and tension tests. As will be pointed out in this section, in addition to mechanical characterization, proper analysis of the data can provide us with information about the nature of CNT-CNT interactions.

As shown in Section 2.4., DMA is commonly used to investigate the viscoelastic response of CNT-polymer composites. Generally it is accepted that an increase in the storage modulus indicates the reinforcing effect of CNTs in a polymer matrix.[67–71] This is based on the fact that strong interactions between CNTs prevent slippage between CNTs and the matrix, further enhancing the elastic energy storage in the sample at sufficiently low strains. Moreover, the variations of the T_g, measured as the temperature corresponding to the maximum loss modulus with CNT content contains valuable information about the ensemble interactions between CNTs and the polymer matrix. For instance, the increase in T_g with CNT content is considered as an indication of the loss of mobility of polymer chains in the presence of CNTs.[67,71] Despite the hindrance effect of CNTs on chain mobility, Hwang et al. reported a reduction in T_g as a function of CNTs in poly(Methyl methacrylate) (PMMA) up to 20 wt% CNTs, when CNTs themselves were grafted with PMMA.[69] The reduction in T_g with CNT content was attributed to the plasticizing effect of the functional groups in the aforementioned matrix. Moreover, they observed a second peak in the loss modulus at ~9 wt% of CNTs, suggestive nonuniform dispersion of CNTs in the composites for 9 wt% CNT content and above, which further facilitates the polymer chain motion.

In addition to the storage modulus and T_g, the shape of the dynamic moduli curves as a function of temperature provides additional clues about the nature of the interactions between CNTs and polymers. For instance, Shaffer and Windle reported a broadening of loss modulus curves by increasing the CNT contents in CNT-Polyvinylalcohol (PVA) to ~60 wt%, which was attributed to the loss of mobility of the unconstrained portions of the PVA chains by adding CNTs.[70]

Despite the information they reveal about the material stiffness and the nature of interactions between CNTs and polymers, DMA experiments can only capture the small strain mechanical response of the sample. Another class of experiments, used to capture both the small deformation (such as modulus) and large deformation (such as strength and toughness) mechanical properties of the CNT composites, is tension tests. Similar to DMA experiments, in tension tests, it is commonly accepted that an increase in the modulus or strength of CNT composites with the addition of CNTs or with proper functionalization of CNTs points to enhanced interaction between CNTs and the matrix due to proper functionalization of CNTs or their uniform dispersion.[67,73,74]

In addition, given the low ductility of typical CNT yarns, the statistical analysis of the mechanical properties, such as strength and modulus, can be instrumental in assessing the average distribution of defects in the as-produced sample. For instance, Kozoil et al. measured the strength of in situ CVD fabricated CNT yarns with varying gage length ranging from 1 to 20 mm (see **Figure 9**)[20,21] to assess the defect density in the samples. At all gage lengths, they observed a peak in strength at around 1 N GPa/g/cm^3 (0.5–1.5 GPa), while at sufficiently low gage length (1–2 mm) another peak appeared at ~5 GPa/g/cm^3 (~9 GPa). The variation of strength with gage length and the peak observed at the smallest gauge length pointed to the presence of defects in the sample that were, on average, on the order of 1–2 mm apart from one another, which controlled the mechanical response of samples with sufficiently large gage length. Moreover, the good correlation between the modulus and strength in all the samples eliminated the possibility of

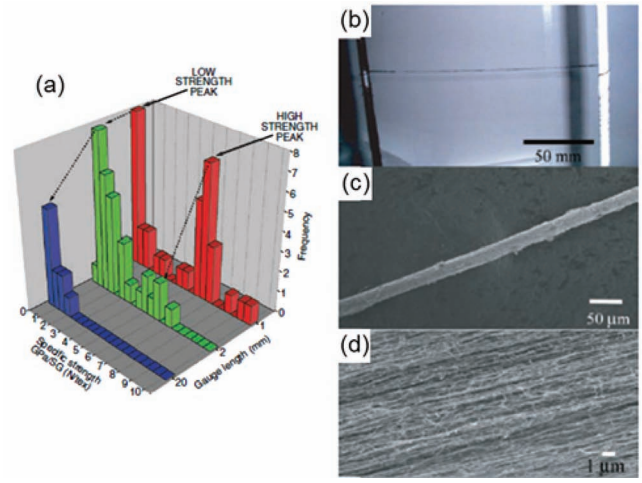

Figure 9. Micro tensile testing of CNT yarns. (a) Histogram of specific strength of in situ CVD spun CNT yarns for multiple gauge lengths. Reprinted with permission from AAAS.[21] (b-d) Optical and SEM images of in situ CVD spun yarns at different length scales. Reprinted with permission from AAAS.[20]

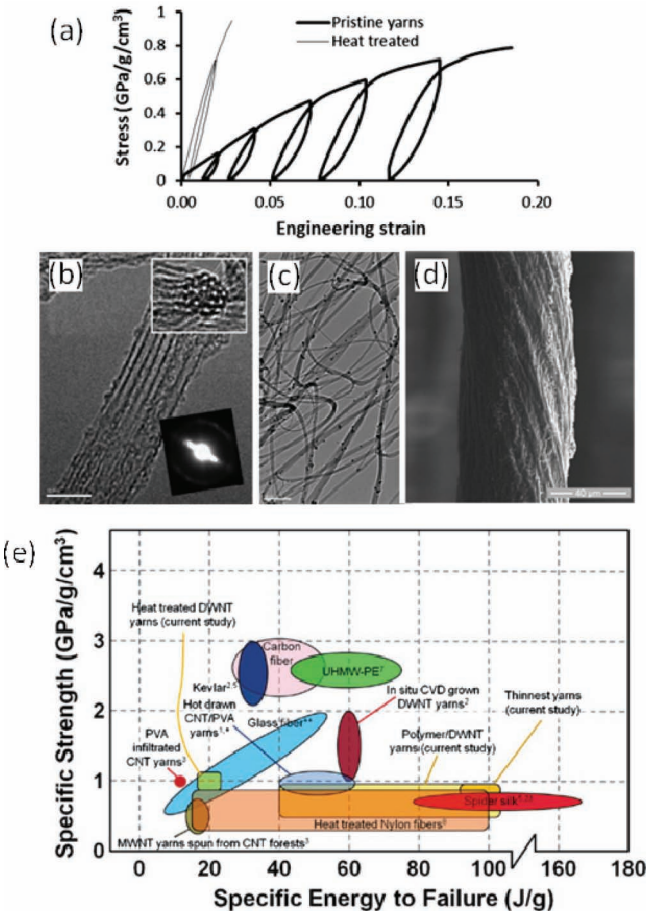

Figure 10. (a) Stress-strain curve of DWNT yarns with and without polymer crosslinking. (b-d) SEM images of DWNT/polymer yarn at different hierarchical length scales. (e) Ashby style plot of specific strength as a function of specific energy-to-failure for advanced yarns and fibers.[23] Adapted with permission,[23] Copyright 2010, American Chemical Society.

the presence of flaws in the sample that would introduce stress concentrations, as the adverse effect of such flaws on strength would be more significant than on the modulus. From these findings they concluded that the defects in the samples were likely due to a lower densification in some parts of the fibers, which affects the modulus and strength similarly.

Baughman et al. pointed to the crucial role of twist in the mechanical behavior of yarns of CNTs, drawn from CVD grown forests of CNTs, to induce transverse forces between constituents to bind CNTs together.[79] As shown by Polarized Raman spectroscopy, this method of drawing of CNTs from CNT forests induces partial alignment between CNTs in the as drawn sheets of CNTs.[111] A combination of CNT alignment and enhanced interactions between CNTs due to twist resulted in yarns with strength close to ~1 GPa (specific strength of ~0.6 GPa/g/cm^3) and toughness as high as ~30 J/g measured in tension, which is comparable to high performance fibers.[112] The role of lateral interactions through polymer coatings has also been revealed by Espinosa and co-workers. They found that yarns with very high volume fraction of DWNT incorporating polymer intermediaries, primarily composed of substituted acrylates formed during CVD growth, exhibited specific strengths in excess of 1 GPa/g/cm^3 and toughness as high as ~100 J/g.[23] These yarns were among the first to achieve simultaneously high specific strengths (higher than the ones previously reported for CNTs) and energies to failure similar to the one of nature's toughest materials, spider silk (see **Figure 10**).

The significant Poisson effect observed in the yarns has been successfully exploited to develop mechanical strain sensors with sensitivities of as high as 0.5 μV/με. The basis of the operation of these electromechanical sensors is the reduction in the volume of yarns upon axial loading, and the consequent reduction in their electric charge capacity.[113] However, it is to be pointed out that the twist has an adverse effect on the modulus of yarns, resulting in yarns with moduli substantially lower than the modulus of their constituents (CNT), due to the loading of CNTs in an inclined direction with respect to the yarn axis.[112]

Tension tests on CNT composites can also been carried out in situ analytical chambers, such as SEM, to visualize the deformation mechanisms of CNT composites. Naraghi *et al.* investigated the mechanical behavior of twisted CNT yarns in situ SEM.[23] They observed significantly high lateral contraction of the yarns in response to axial loading and Poisson ratios of as high as 1, mostly due to the twisted structure of the yarns, similar in nature to the giant Possion effect observed for axially loaded CNT yarns spun from CVD grown forests of CNTs.[19,79,112] As explained in[79] and experimentally demonstrated in,[23] the giant Poisson effect is rooted in the twisted morphology of the yarn and the consequent "unwinding" of its helical structure upon axial loading. This effect can result in volume loss of the sample and its lateral contraction during axial loading, thus enhancing the interactions between CNTs. Together with enhanced alignment of CNTs during axial loading, the enhanced load transfer between CNTs can account for the increase of elastic modulus

of the yarns with plastic strain.[23,79] Through their in situ SEM experiments on yarns of DWNT bundles with an inherent polymer coating developed in the CVD reactor, Naraghi et al. demonstrated that the yarns accommodate the applied deformation by both reorientation of the network of CNTs (due to the yarn twisted morphology) and the network stretching, with similar contributions from each component.[23] Moreover, by coupling macroscale tension experiments on yarns with in situ SEM tension tests on DWNT bundles, they demonstrated that only a small portion of the total energy given to the system by the tension test apparatus is stored in CNTs, while most of it is dissipated by the shear interactions between CNT and the inherent polymer coating. Continuum and analytical models can also be applied to predict macroscopic fiber and yarn mechanical properties based on experimental data and microscopic simulations. Vilatela et al. recently developed a model of the strength of aligned CNT yarns and identified optimization parameters of the subunits of the yarns which included CNT length and interlayer shear strength.[114] In particular it was predicted that by using large diameter CNTs with few walls the degree of contact between adjacent CNTs could be increased leading to higher strength.

In addition to the measurement of mechanical properties, the shape of stress-strain curves obtained in tension tests can give insights into deformation mechanisms involved in CNT composites and the ensemble behavior of the CNT-polymer chain interactions. For instance, the lack of plastic deformation and the "wave-like pattern" of the curves, in layer by layer deposited CNT composites with as high as 50 wt% CNTs, was suggestive of the uncoiling of the entangled polymer chains, followed by their rupture.[72]

4. Concluding Remarks

The emergence of hierarchical design in carbon-based composites is showing great promise in the development of mechanically superior and multifunctional materials. Progress in this field relies heavily on understanding both the mechanical behavior of the constituents and interactions between them at multiple length scales, a challenge that has been addressed in part by mulitscale experiments. At the nanoscale, the application of AFM and in situ TEM methods have been used to measure the intrinsic mechanical properties of promising building blocks, most notably the strength and stiffness of CNT shells[11,12] and graphene sheets,[115] which are now known to a high degree of certainty. The same, however, cannot be said for the mechanical interactions between constituent such as adjacent CNTs or graphene sheets. While experimental techniques have provided a great deal of insight into the nature of these shear interactions, there remain large variations in reported measurements, one example being the shear strength measured for adjacent CNT shells (see Table 2). One approach to engineering these interfaces through crosslinking that has proven to be a promising direction is particle irradiation. Irradiation induced crosslinking between adjacent tubes and shells of CNTs has been demonstrated to improve effective mechanical properties, such as strength and stiffness, by orders of magnitude,[12,18,55] however this approach has not yet been demonstrated in macroscopic fibers or yarns due to difficulties in uniformly irradiating large quantities of materials. Despite the lack of a complete understanding of the behavior at such intermediate length scales a great deal of progress has already been made in developing macroscopic materials for end user applications. CNT based fibers and yarns, which have benefited from engineered interfacial interactions and geometrical parameters such as alignment and twist, have emerged, exhibiting mechanical properties superior to more commonly available materials such as steels and Kevlar.[21,23,116] In addition, the multi-functionality of macroscopic fibers that incorporate CNTs and graphene sheets has emerged recently, which addresses the growing need for novel technologies with energy applications. Initial demonstrations include yarns of superconductors, lithium-ion battery materials, and titanium dioxide for photocatalysis.[24]

The next significant leaps in understanding of hierarchical carbon-based materials can highly benefit from the coupling of multiscale experimental tools with computation approaches. Multiscale simulations on the class of materials discussed in this article are beginning to fill in some of the gaps in our understanding of their mechanical behavior. In the case of natural materials, such as tendon and spider silk, multiscale simulations have been instrumental in elucidating how the hierarchical structures and interactions between constituents contribute to the impressive macroscopic properties.[1,3] Moreover, a great deal of activity is now focused on applying these lessons of nature to materials engineered out of carbon constituents.

The modeling of carbon-based hierarchical materials requires the development and coupling of models across a number of length scales. At the nanoscale, density functional theory (DFT) simulations have predicted the intrinsic mechanical properties of CNTs[117,118] and graphene[119] and can be extended to characterize the interaction of individual crosslinking elements. At intermediate length scales, molecular mechanics (MM) and molecular dynamics (MD) simulations can be applied to investigate load transfer between adjacent graphitic sheets in larger systems. In particular, MM and MD studies of CNT bundles have provided insights into the nature of shear interactions and load transfer mechanisms between adjacent CNTs within bundles.[62,120] In this case, the MM potentials used (e.g., modified second generation Tersoff-Brenner[121]) can be directly validated by comparison to DFT calculations.[12] Similar studies also include simulations that incorporate many crosslinking elements such as covalent crosslinking defects that occur as a result of electron irradiation.[100] For MD simulations the application of ReaxFF reactive force fields has proven to be powerful in developing an understanding of carbon materials.[122–124] These have extended from studies of the catalytic formation of CNTs,[123,124] to the fracture properties of individual graphene sheets.[122] On the other hand, networks of many interacting CNTs and graphene sheets, such as crosslinked bundles of tens to hundreds of CNTs, are typically too large and computationally costly to be simulated by traditional MM or MD, therefore simulation approaches that use coarse grain elements can be applied.[101] Here individual mechanical properties of the elements, as well as interaction parameters such as cohesive energies between

adjacent constituents, are input from independent DFT and MM/MD calculations. Finally, continuum and analytical models can predict macroscopic fiber and yarn properties. Example are the recent work of Espinosa and co-workers[17] and Vilatela et al.,[114] in which the mechanical properties of highly aligned CNT yarns were modeled based on experimental data and molecular dynamic simulations. Using their model, Vilatela et al. identified critical steps in the enhancement of the mechanical behavior of CNT yarns, for instance by utilizing thick CNTs with few shells that can "autocollapse," increasing the contact area between adjacent CNTs.

A combination of existing multiscale experimental and theoretical tools alone, however, will not be sufficient to fully explore the potential of hierarchical carbon materials. Novel tools and materials also need to be explored and developed. For example the in situ electron microscopy testing capabilities that have been discussed earlier are typically quasi static and restricted to extremely low temporal resolution due to limitations in image capturing. However, many applications, in particular the development of CNT/graphene based bullet proof armors, will require a better understanding of dynamic failure properties. Furthermore, we would expect large strain rate dependence of CNT based fibers and yarns. One approach to investigate such dependencies at the nanoscale would be the application of dynamic TEMs (DTEM) to study deformation and failure in carbon-based materials. The viability and potential technical capabilities of DTEM have been discussed recently,[125] and it has already been applied to reveal the dynamic propagation of reaction fronts in layered materials with nanosecond resolution.[126] However, its application to atomic scale studies of CNT and graphene based materials will require further improvements in overcoming the space charge effects, which limit the spatial resolution in current DTEM experiments. Moreover, force and strain measurement techniques in situ TEM and SEM on nanoscale samples, which are mostly based on the deflection measurement of cantilevers, should be augmented, for instance by all electronic in situ SEM/TEM measurements as the ones reported in.[34–36] By using such improved systems, load and strain resolution can be substantially enhanced, and stiff load sensors can be incorporated, for instance, in an attempt to stably capture weak interactions between CNTs (see Section 3.1).

Along with advancing novel methods of measuring material properties of CNT/graphene hierarchical materials, researchers must also continue advancing the study of both complementary and alternative materials. One example is the development of CNT composites incorporating strong materials such as Kevlar, which can form strong π-stacking interactions with unfunctionalized tubes. This approach has been recently demonstrated to produce CNT reinforced Kevlar composites with strength as high as 6 GPa and modulus as high as 200 GPa.[127] However, these values of mechanical properties, while remarkable, are still a small fraction of the properties of CNTs, thus, demanding future research in this area. Another material system that has attracted the attention of many researchers, is non-carbon-based building blocks such as boron nitride nanotubes and sheets. Boron nitride, also known as "white graphene," has a similar 2D hexagonal structure as graphene and has attracted a great deal of attention recently for a number of reasons including its remarkably high mechanical properties (strength ~ 30 GPa and modulus ~ 900 GPa[128]), comparable to those of CNTs, and superior thermal stability.

Received: December 20, 2011
Published online: May 11, 2012

[1] M. J. Buehler, *Proceed. Nat. Acad. Sci.* **2006**, *103*, 12285.
[2] H. D. Espinosa, J. E. Rim, F. Barthelat, M. J. Buehler, *Progress in Materials Science* **2009**. *54*, 1059.
[3] S. Keten, Z. Xu, B. Ihle, M. J. Buehler, *Nat. Mater.* **2010**, *9*, 359.
[4] M. Meyers, P. Chen, Y. Lin, Y. Seki, *Progress in Materials Science* **2008**, *53*, 1.
[5] F. G. Omenetto, D. L. Kaplan, *Science* **2010**, *329*, 528.
[6] U. Wegst, M. Ashby, *Philosophical Magazine* **2004**, *84*, 2167.
[7] A. Nova, S. Keten, N. M. Pugno, A. Redaelli, M. J. Buehler, *Nano Letters* **2010**. *10*, 2626.
[8] T. Giesa, M. Arslan, N. M. Pugno, M. J. Buehler, *Nano Letters* **2011**, *11*, 5038.
[9] H. D. Espinosa, A. L. Juster, F. J. Latourte, O. Y. Loh, D. Gregoire, P. D. Zavattieri, *Nature Communications* **2011**, *2*.
[10] M. Elices, G. V. Guinea, G. R. Plaza, C. Karatzas, C. Riekel, F. Agullo-Rueda, R. Daza, J. Perez-Rigueiro, *Macromolecules* **2011**, *44*, 1166.
[11] M. F. Yu, O. Lourie, M. J. Dyer, K. Moloni, T. F. Kelly, R. S. Ruoff, *Science* **2000**, *287*, 637.
[12] B. Peng, M. Locascio, P. Zapol, S. Li, S. L. Mielke, G. C. Schatz, H. D. Espinosa, *Nature Nanotechnology* **2008**, *3*, 626.
[13] C. W. Lee, X. Wei, J. W. Kysar, J. Hone, *Science* **2008**, *321*, 385.
[14] H. Aslan, N. Kimelman-Bleich, G. Pelled, D. Gazit, *Journal of Clinical Investigation* **2008,** *118,* 439.
[15] A. Gautieri, S. Vesentini, A. Redaelli, M. J. Buehler, *Nano Letters* **2011**, *11*, 757.
[16] Y. L. Sun, Z.-P. Luo, A. Fertala, K.-N. An, *J Biomech* **2004**, *37*, 1665.
[17] X. Wei, M. Naraghi, H. D. Espinosa, ACS Nano, **2012**, *6*, 2333.
[18] T. Filleter, R. A. Berrnal, S. Li, H. D. Espinosa, *Adv. Mater.* **2011**, *23*, 2855.
[19] A. B. Dalton, S. Collins, E. Munoz, J. M. Razal, V. H. Ebron, J. P. Ferraris, J. N. Coleman, B. G. Kim, R. H. Baughman, *Nature* **2003**, *423*, 703.
[20] Y.-L. Li, I. Kinloch, A. Windle, *Science* **2004**, *304*, 276.
[21] K. Koziol, J. Vilatela, A. Moisala, M. Motta, P. Cunniff, M. Sennett, A. Windle, *Science* **2007**, *318*, 1892.
[22] M. Motta, A. Moisala, I. A. Kinloch, A. H. Windle, *Adv. Mater.* **2007**, *19*, 3721.
[23] M. Naraghi, T. Filleter, A. Moravsky, M. Locasio, R. O. Loufty, H. D. Espinosa, *ACS Nano* **2010**, *4*, 6463.
[24] M. D. Lima, S. L. Fang, X. Lepro, C. Lewis, R. Ovalle-Robles, J. Carretero-Gonzalez, E. Castillo-Martinez, M. E. Kozlov, J. Y. Oh, N. Rawat, C. S. Haines, M. H. Haque, V. Aare, S. Stoughton, A. A. Zakhidov, R. H. Baughman, *Science* **2011**, *331*, 51.
[25] A. E. Aliev, J. Y. Oh, M. E. Kozlov, A. A. Kuznetsov, S. L. Fang, A. F. Fonseca, R. Ovalle, M. D. Lima, M. H. Haque, Y. N. Gartstein, M. Zhang, A. A. Zakhidov, R. H. Baughman, *Science* **2009**, *323*, 1575.
[26] S. Stankovich, D. A. Dikin, G. H. B. Dommett, K. M. Kohlhaas, E. J. Zimney, E. A. Stach, R. D. Piner, S. T. Nguyen, R. S. Ruoff, *Nature* **2006**, *442*, 282–286.
[27] D. A. Dikin, S. Stankovich, E. J. Zimney, R. D. Piner, G. H. B. Dommett, G. Evmenenko, S. B. T. Nguyen, R. S. Ruoff, *Nature* **2007**, *448*, 457–460.
[28] J. Cumings, A. Zettl, *Science* **2000**, *289*, 602.
[29] W. J. Ma, L. Q. Liu, R. Yang, T. H. Zhang, Z. Zhang, L. Song, Y. Ren, J. Shen, Z. Q. Niu, W. Y. Zhou, S. S. Xie, *Advanced Materials* **2009**, *21*, 603.

[30] E. J. Garcia, A. J. Hart, B. L. Wardle, A. H. Slocum, *Advanced Materials* **2007**, *19*, 2151.
[31] S. Iijima, *Nature* **1991**, *354*, 56.
[32] C.K. Jannik, C. Meyer, R. Erni, M. D. Rossell, M. F. Crommie, A. Zettl, *Nano Letters* **2008**, *8*, 3582–3586.
[33] M. Legros, D. S. Gianola, C. Motz, *MRS Bulletin* **2010**, *35*, 354.
[34] M. A. Haque, M. T. A. Saif, *Experimental Mechanics* **2003**, *43*, 248.
[35] Y. Zhu, N. Moldovan, H. D. Espinosa, *Applied Physics Letters* **2005**, *86,* 013506.
[36] Y. Zhu, A. Corigliano, H. D. Espinosa, *Journal of Micromechanics and Microengineering* **2006**, *16*, 242.
[37] A. M. Minor, S. A. S. Asif, Z. W. Shan, E. A. Stach, E. Cryrankowski, T. J. Wyrobek, O. L. Warren, *Nature Materials* **2006**, *5*, 697.
[38] Z. W. Shan, R. K. Mishra, S. A. S. Asif, O. L. Warren, A. M. Minor, *Nature Materials* **2008**, *7*, 115.
[39] M. Locascio, B. Peng, P. Zapol, Y. Zhu, S. Li, T. Belytschko, H. D. Espinosa, *Experimental Mechanics* **2009**, *49*, 169.
[40] R. Agrawal, B. Peng, E. E. Gdoutos, H. D. Espinosa, *Nano Letters* **2008**, *8*, 3668.
[41] Y. Zhu, H. D. Espinosa, *Proc. Natl. Acad. Sci. USA*, **2005**, *102*, 14503.
[42] P. M. Osterberg, S. D. Senturia, *Journal of Microelectromechanical Systems* **1997**, *6*, 107.
[43] R. Ballarini, R. L. Mullen, Y. Yin, H. Kahn, S. Stemmer, A. H. Heuer, *Journal of Materials Research* **1997**, *12*, 915.
[44] M. P. de Boer, B. D. Jensen, F. Bitsie, *Materials and Device Characterization in Micromachining Ii* **1999**, *3875*, 97.
[45] M. A. Haque, M. T. A. Saif, *Journal of Microelectromechanical Systems* **2001**, *10*, 146.
[46] M. A. Haque, M.T.A. Saif, *Journal of Materials Research* **2005**, *20*, 1769.
[47] M. A. Haque, H. D. Espinosa, H. J. Lee, *MRS Bulletin* **2010**, *35*, 375.
[48] J. W. Suk, R. D. Piner, J. An, R. S. Ruoff, *ACS Nano* **2010**, *4*, 6557.
[49] H. D. Espinosa, B. C. Prorok, *Journal of Materials Science* **2003**, *38*, 4125.
[50] H. D. Espinosa, B. C. Prorok, B. Peng, *Journal of the Mechanics and Physics of Solids* **2004**, *52*, 667.
[51] H. D. Espinosa, B. C. Prorok, M. Fischer, *Journal of the Mechanics and Physics of Solids* **2003**, *51*, 47.
[52] T. Filleter, J. L. McChesney, A. Bostwick, E. Rotenberg, K. V. Emtsev, T. Seyller, K. Horn, R. Bennewitz, *Physical Review Letters* **2009**, *102*, 086102.
[53] Q. Y. Li, C. Lee, R. W. Carpick, J. Hone, *Physica Status Solidi B-Basic Solid State Physics* **2010**, *247*, 2909.
[54] M. F. Yu, B. Files, S. Arepalli, R. Ruoff, *Physical Review Letters* **2000**, *84*, 5552.
[55] A. Kis, G. Csanyi, J. P. Salvetat, T. N. Lee, E. Couteau, A. J. Kulik, W. Benoit, J. Brugger, L. Forro, *Nature Materials* **2004**, *3*, 153.
[56] *Scanning Probe Microscopy: The Lab on a Tip* (Eds: E. Meyer, H. Hug, R. Bennewitz), Springer-Verlag, Berlin **2004**.
[57] M. F. Yu, B.I. Yakobson, R. S. Ruoff, *Journal of Physical Chemistry B* **2000**, *104*, 8764.
[58] I. Kaplan-Ashiri, S. R. Cohen, N. Apter, Y. K. Wang, G. Seifert, H. D. Wagner, R. Tenne, *Journal of Physical Chemistry C* **2007**, *111*, 8432.
[59] B. Bhushan, X. Ling, A. Jungen, C. Hierold, *Physical Review B* **2008**, *77*, 165428.
[60] M. Naraghi, G. Bratzel, T. Filleter, Z. An, X. Wei, S. T. Nguyen, M. J. Buehler, H. D. Espinosa, unpublished.
[61] O. Suekane, A. Nagataki, H. Mori, Y. Nakayama, *Applied Physics Express* **2008**, *1*, 064001.
[62] T. Filleter, S. Yockel, M. Naraghi, J. T. Paci, O. C. Compton, M. L. Mayes, S. T. Nguyen, G. C. Schatz, H. D. Espinosa, *Nano Lett.* **2012**, *12*, 732.
[63] T. Y. Yang, Z. R. Zhou, H. Fan, K. Liao, *Applied Physics Letters* **2008**, *93*, 041914.
[64] S. H. Syue, S. Y. Lu, W. K. Hsu, H. C. Shih, *Applied Physics Letters* **2006**, *89*, 163115.
[65] J. N. Coleman, U. Khan, W. J. Blau, Y. K. Gun'ko, *Carbon* **2006**, *44*, 1624.
[66] Z. Spitalsky, D. Tasis, K. Papagelis, C. Galiotis, *Progress in Polymer Science* **2010**, *35*, 357.
[67] J. W. Yang, J. H. Hu, C. C. Wang, Y. J. Qin, Z. X. Guo, *Macromolecular Materials and Engineering* **2004**, *289*, 828.
[68] Z. Wang, Z. Y. Liang, B. Wang, C. Zhang, L. Kramer, *Composites Part a-Applied Science and Manufacturing* **2004**, *35*, 1225.
[69] G. L. Hwang, Y. T. Shieh, K. C. Hwang, *Advanced Functional Materials* **2004**, *14*, 487.
[70] M. S. P. Shaffer, A. H. Windle, *Advanced Materials* **1999**, *11*, 937.
[71] Y. T. Shieh, G. L. Liu, Y. K. Twu, T. L. Wang, C. H. Yang, *Journal of Polymer Science Part B-Polymer Physics* **2010**, *48*, 145.
[72] A. A. Mamedov, N. A. Kotov, M. Prato, D. M. Guldi, J. P. Wicksted, A. Hirsch, *Nature Materials* **2002**, *1*, 190.
[73] N. G. Sahoo, H. K. F. Cheng, J. W. Cai, L. Li, S. H. Chan, J. H. Zhao, S. Z. Yu, *Materials Chemistry and Physics* **2009**, *117*, 313.
[74] K. Yang, M. Y. Gu, Y. P. Guo, X. F. Pan, G. H. Mu, *Carbon* **2009**, *47*, 1723.
[75] L. Q. Liu, D. Tasis, M. Prato, H. D. Wagner, *Advanced Materials* **2007**, *19*, 1228.
[76] C. A. Cooper, R. J. Young, M. Halsall, *Composites Part a-Applied Science and Manufacturing* **2001**, *32*, 401.
[77] M. F. Mu, S. Osswald, Y. Gogotsi, K. I. Winey, *Nanotechnology* **2009**, *20*, 335703.
[78] M. S. Dresselhaus, G. Dresselhaus, R. Saito, A. Jorio, *Physics Reports* **2005**, *409*, 47.
[79] M. Zhang, K. R. Atkinson, R. H. Baughman, *Science* **2004**, *306*, 1358.
[80] T. X. Liu, I. Y. Phang, L. Shen, S. Y. Chow, W. D. Zhang, *Macromolecules* **2004**, *37*, 7214.
[81] X. F. Li, K. T. Lau, Y. S. Yin, *Composites Science and Technology* **2008**, *68*, 2876.
[82] D. Lee, T. H. Cui, *Nanotechnology* **2011**, *22*, 165601.
[83] M. Minary-Jolandan, M. F. Yu, *Journal of Applied Physics* **2008**, *103*, 073516.
[84] M. Mayor, H. B. Weber, J. Reichert, M. Elbing, C. von Hanisch, D. Beckmann, M. Fischer, *Angew. Chem. Int.* **2003**, *42*, 5834.
[85] S. R. Bakshi, R. G. Batista, A. Agarwal, *Composites Part A* **2009**, *40*, 1311.
[86] G. M. Pharr, W. C. Oliver, F. R. Brotzen, *Journal of Materials Research* **1992**, *7*, 613.
[87] A. Kis, A. Zettl, *Philosophical Transactions of the Royal Society A* **2008**, *366*, 1591.
[88] A. Kis, K. Jensen, S. Aloni, W. Mickelson, A. Zettl, *Physical Review Letters* **2006**, *97*, 025501.
[89] N. G. Chopra, L. X. Benedict, V. H. Crespi, M. L. Cohen, S. G. Louie, A. Zettl, *Nature* **1995**, *377*, 135.
[90] C. H. Ke, M. Zheng, G. W. Zhou, W. L. Cui, N. Pugno, R. N. Miles, *Small* **2010**, *6*, 438.
[91] R.J. Good, L.A. Girifalco, G. Kraus, *Journal of Physical Chemistry* **1958**, *62*, 1418.
[92] M. Ishikawa, R. Harada, N. Sasaki, K. Miura, *Applied Physics Letters* **2008**, *93*, 083122.
[93] B. Bhushan, *Introduction to Tribology*, John Wiley & Sons, NY, USA **2002**.
[94] M. Dienwiebel, G. S. Verhoeven, N. Pradeep, J. W. M. Frenken, J. A. Heimberg, H. W. Zandbergen, *Physical Review Letters* **2004**, *92*, 126101.
[95] L. A. Girifalco, R. A. Lad, *Journal of Chemical Physics* **1956**, *25*, 693.

[96] R. Zacharia, H. Ulbricht, T. Hertel, *Physical Review B* **2004**, *69*, 115424.
[97] R. Zacharia, H. Ulbricht, T. Hertel, *Physical Review B* **2004**, *69*, 155406.
[98] F. Banhart, *Reports on Progress in Physics* **1999**, *62*, 1181.
[99] R. H. Telling, C. P. Ewels, A. A. El Barbary, M. I. Heggie, *Nature Materials* **2003**, *2*, 333.
[100] C. F. Cornwell, C. R. Welch, *Journal of Chemical Physics* **2011**, *134*, 204708.
[101] G. H. Bratzel, S. W. Cranford, H. Espinosa, M. J. Buehler, *Journal of Materials Chemistry* **2010**, *20*, 10465.
[102] M. B. Cristina Gómez-Navarro, Klaus Kern, *Nano Letters* **2008**, *8*, 2045.
[103] K. Erickson, R. Erni, Z. Lee, N. Alem, W. Gannett, A. Zettl, *Advanced Materials* **2010**, *22*, 4467.
[104] O. C. Compton, B. Jain, D. A. Dikin, A. Abouimrane, K. Amine, S. T. Nguyen, *ACS Nano* **2011**, 5, 4380.
[105] S. Park, K. S. Lee, G. Bozoklu, W. Cai, S. T. Nguyen, R. S. Ruoff', *ACS Nano* **2008**, *2*, 572.
[106] D. A. D. Sungjin Park, SonBinh T. Nguyen, Rodney S. Ruoff, *J. Phys. Chem. C. Lett.* **2009**, *113*, 15801.
[107] S. B. Cronin, A. K. Swan, M. S. Unlu, B. B. Goldberg, M. S. Dresselhaus, M. Tinkham, *Physical Review B* **2005**, *72*, 035425.
[108] R. J. Cannara, M. J. Brukman, R. W. Carpick, *Review of Scientific Instruments* **2005**, *76*, 053706.
[109] A. Misra, J.R. Raney, L. De Nardo, A. E. Craig, C. Daraio, *ACS Nano* **2011**, *5*, 7713.
[110] A. Misra, J. R. Raney, A. E. Craig, C. Daraio, *Nanotechnology* **2011**, *22*, 425705.
[111] M. Zhang, S. L. Fang, A. A. Zakhidov, S. B. Lee, A. E. Aliev, C. D. Williams, K. R. Atkinson, R. H. Baughman, *Science* **2005**, *309*, 1215.
[112] K. R. Atkinson, S. C. Hawkins, C. Huynh, C. Skourtis, J. Dai, M. Zhang, S. L. Fang, A. A. Zakhidov, S. B. Lee, A. E. Aliev, C. D. Williams, R. H. Baughman, *Physica B-Condensed Matter* **2007**, *394*, 339.
[113] T. Mirfakhrai, J. Oh, M. E. Kozlov, S. L. Fang, M. Zhang, R. H. Baughman, J. D. W. Madden, *IEEE-Asme Transactions on Mechatronics* **2011**, *16*, 90.
[114] J. J. Vilatela, J. A. Elliott, A. H. Windle, *ACS Nano* **2011**, *5*, 1921.
[115] C. Lee, X. Wei, J. W. Kysar, J. Hone, *Science* **2008**, *321*, 385.
[116] M. Zhang, K. R. Atkinson, R. H. Baughman, *Science* **2004**, *306*, 1358.
[117] S. Ogata, Y. Shibutani, *Physical Review B* **2003**, *68*, 165409.
[118] T. Ozaki, Y. Iwasa, T. Mitani, *Physical Review Letters* **2000**, *84*, 1712.
[119] F. Liu, P. M. Ming, J. Li, *Physical Review B* **2007**, *76*, 064120.
[120] D. Qian, W. K. Liu, R. S. Ruoff, *Comp. Sci. Technol.* **2003**, *63*, 1561.
[121] D. W. Brenner, O. A. Shenderova, J. A. Harrison, S. J. Stuart, B. Ni, S. B. Sinnott, *Journal of Physics: Condensed Matter* **2002**, *14*, 783.
[122] D. Sen, K. S. Novoselov, P. M. Reis, M. J. Buehler, *Small* **2010**, *6*, 1108.
[123] E. C. Neyts, Y. Shibuta, A. C. T. van Duin, A. Bogaerts, *ACS Nano* **2010**, *4*, 6665.
[124] K. Nielson, A. Van Duin, J. Oxgaard, W. Deng, W. Goddard III, *J. Phys. Chem. A* **2005**, *109*, 493.
[125] M. R. Armstrong, K. Boyden, N. D. Browning, G. H. Campbell, J. D. Colvin, W. J. DeHope, A. M. Frank, D.J. Gibson, F. Hartemann, J. S. Kim, W. E. King, T. B. LaGrange, B. J. Pyke, B. W. Reed, R. M. Shuttlesworth, B. C. Stuart, B. R. Torralva, *Ultramicroscopy* **2007**, *107*, 356.
[126] J. S. Kim, T. LaGrange, B. W. Reed, M. L. Taheri, M. R. Armstrong, W. E. King, N. D. Browning, G. H. Campbell, *Science* **2008**, *321*, 1472.
[127] I. O'Connor, H. Hayden, J. N. Coleman, Y. K. Gun'ko, *Small* **2009**, *5*, 466.
[128] X. L. Wei, M. S. Wang, Y. Bando, D. Golberg, *Advanced Materials* **2010**, *22*, 4895.